Asian Power Electronics Journal

PERC, HK PolyU

First edition Dec. 2015 Printed in Hong Kong by Reprographic Unit
The Hong Kong Polytechnic University

Published by

Power Electronics Research Centre
The Hong Kong Polytechnic University
Hung Hom, Kowloon, Hong Kong

ISSN 1995-1051

Disclaimer

Any opinions, findings, conclusions or recommendations expressed in this material/event do not reflect the views of The Hong Kong Polytechnic University

Editorial board

Table of Content

Bootstrap Gate Driver and Output Filter of An SC-based Multilevel Inverter for Aircraft APU

Yuanmao YE ,K.W.Eric CHENG, N.C. Cheung

Power Electronics Research Centre, Department of Electrical Engineering, The Hong Kong Polytechnic University, Hong Kong
yuanmao.ye@connect.polyu.hk, eeecheng@polyu.edu.hk, norbert.cheung@polyu.edu.hk

Abstract–The objective of this paper is to propose a gate drive circuit and an output filter of a switched-capacitor–based multilevel inverter for aircraft APU. With the bootstrap methodology, only one voltage source is required to power the gate driver of all switches used in the multilevel inverter. With the LC filter, this inverter is capable of providing a pure sinusoidal output voltage waveform. Finally, the performance of the proposed multilevel inverter is evaluated with simulation results and experimental results of an eleven-level prototype inverter.

Keywords–Multilevel inverter, switched-capacitor, bootstrap capacitor driver, sinusoidal PWM.

I. INTRODUCTION

Aircrafts requires an auxiliary power unit (APU) to produce high frequency alternating current, usually 400 Hz. To obtain an output waveform as much as sinusoidal shape, multilevel inverter technique has been an alternative of conventional 2-level inverter. It is well known that the more the levels of an inverter, the more near sinusoidal its output voltage is. It also means the more power semiconductors and voltage sources or capacitors are required. Consequently, one of the key technologies for multilevel inverters is to use less components and simpler structures to obtain the more levels of output voltages.

The conventional multilevel inverters can be divided into three categories [1]: neutral-point-clamped [2], flying capacitors [3], and the H-bridge cascade [4]. One of their common drawbacks is that an excessive number of power semiconductor switches and capacitor sources employed that leads to the complex structure and higher power loss.

In the literature [5], a novel multilevel inverter is presented for high frequency applications. It is made up of a novel DC-DC multilevel converter and an H-bridge as shown in Fig.1. The key point of this inverter is the DC-DC conversion section which consists of multiple switched-capacitor (SC) cells. Each cell employs only one capacitor, one active switch and two diodes. The number of *n-1* SC cells can compose an *n*-level DC-DC converter. They are connected to an H-bridge, a *(2n+1)*-level inverter can be easily derived. The structure is very simple and fewer components are required.

In order to promote this novel multilevel inverter for industrial applications, a simple gate drive circuit is developed by using bootstrap technique in this paper. It means that only one power supply is required to power the gate drive circuit for all switches employed in this inverter. This design philosophy contributes the small size and cost-effectiveness of the inverter.

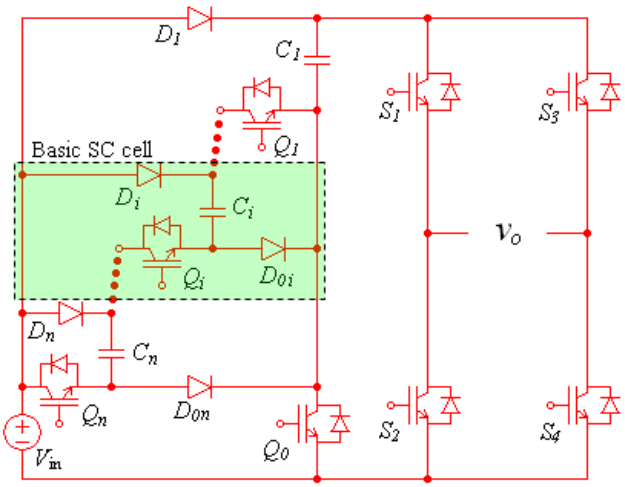

Fig.1: The multilevel inverter presented in [5]

To develop a pure sinusoidal output voltage waveform, an LC filter is added on the output terminal of this multilevel inverter in this paper.

Both simulation and experimental results of a seven-level inverter prototype are provided to evaluate the performance of the inverter.

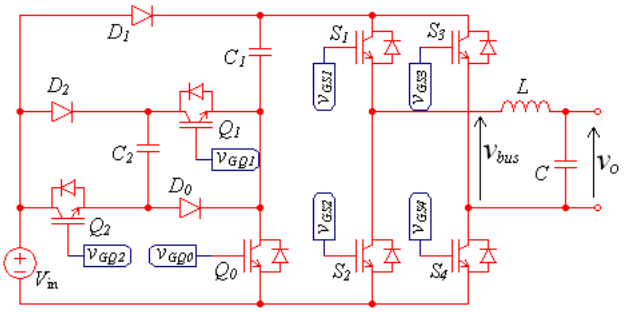

Fig.2: The seven-level topology of the multilevel inverter

II. CIRCUIT DESCRIPTION AND STATES ANALYSIS

1. Circuit Description

Fig.2 shows the topology of proposed inverter in seven levels. It is composed of a three-level DC-DC converter, a full bridge and an output low-pass filter. As mentioned before, the key point of the seven-level inverter is the section of DC-DC converter which consists of three active switches Q_0, Q_1 and Q_2, three diodes D_1, D_2 and D_{02}, and two capacitors C_1 and C_2. With different control strategies for the three active switches, the DC-DC conversion section is capable of converting the input voltage V_{in} in different levels, including $3V_{in}$, $2V_{in}$ and V_{in}. Like many other multilevel inverters aforementioned, the proposed

inverter also includes an inverter bridge which employs four active switches S_1~S_4, and an output LC filter used for filtering higher harmonics.

2. States analysis

As mentioned before, with different control strategies, the circuit section of multilevel DC-DC converter of the proposed inverter is capable of converting the input voltage V_{in} in different levels. For the seven-level inverter as shown in Fig.2, there are three levels that can be produced by the multilevel converter section, including the levels of V_{in}, $2V_{in}$ and $3V_{in}$. With the combination of the operation of the inverter bridge, the inverter can provide seven levels of voltage: $3V_{in}$, $2V_{in}$, V_{in}, 0, $-V_{in}$, $-2V_{in}$ and $-3V_{in}$.

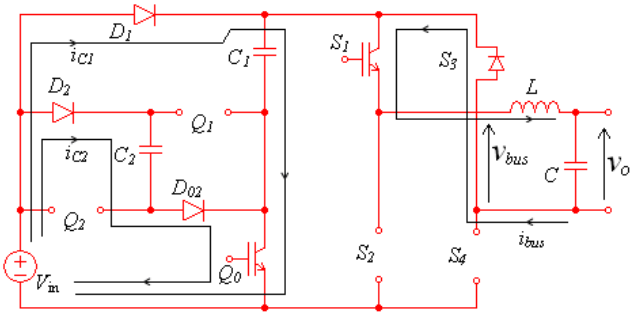

a. the zero level output

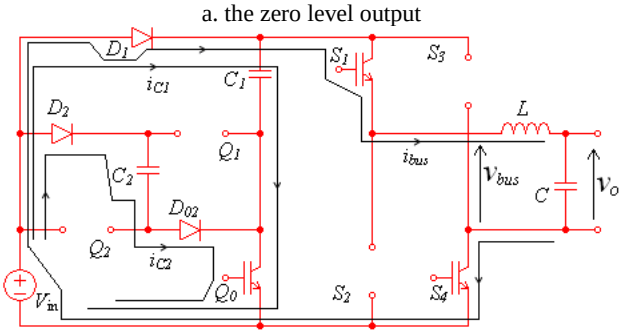

b. the level of V_{in} output

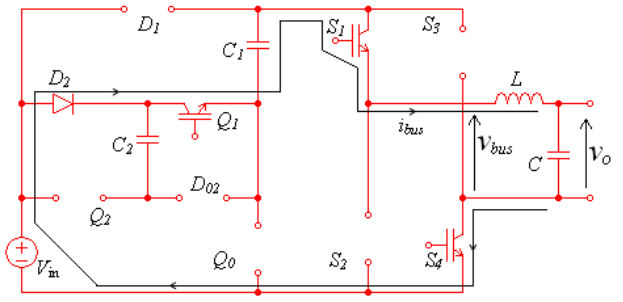

c. the level of $2V_{in}$ output

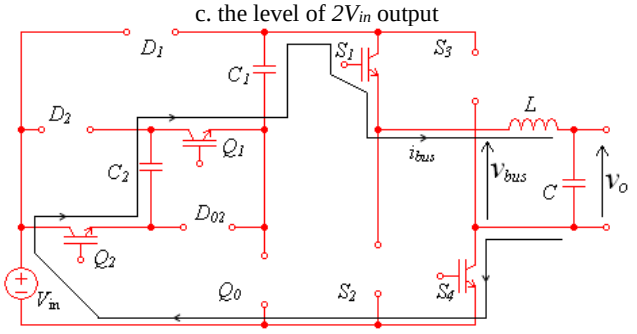

d. the level of $3V_{in}$ output

Fig.3: Working states for the proposed inverter

Specifically, when the switch Q_0 is turned ON and Q_1 and Q_2 being OFF, V_{in}, D_1, C_1 and Q_0 form a closed loop and C_1 is charged by input power V_{in}. And another closed loop is formed by V_{in}, D_2, C_2, D_{02} and Q_0, and C_2 is also charged by V_{in}. In this case, when the switch S_1 is turned ON and other switches in the H-bridge maintains the OFF state as shown in Fig.3a, the output bus voltage v_{bus} is equal to 0. But if the switch S_4 is turned ON as well as shown in Fig.3b, the bus voltage will change to V_{in}. Of course, when the switch S_2 is turned ON, and S_1 and S_4 maintain OFF state, another 0 level and $-V_{in}$ could be produced by being OFF or ON of S_3.

In the DC-DC conversion section, when the switch Q_1 is turned ON and other switches are OFF, the capacitor C_1 is connected in series with input power V_{in} through Q_1 and D_2 and the DC-DC converter section output the voltage level of $V_{in}+V_{C1}$. Assuming the capacitance of C_1 is large enough, the $2V_{in}$ level can be produced by being ON of S_1, S_4 and OFF of S_2 and S_3 as shown in Fig.3c. Similarly, when S_1 and S_4 are turned OFF and S_2, S_3 are turned ON, the level of $-2V_{in}$ can be produced as the bus voltage v_{bus}. When Q_1 and Q_2 are turned ON simultaneously while Q_0 being OFF, capacitors C_1, C_2 and input source V_{in} are connected in series by switches Q_1 and Q_2. Under the condition of the values of C_1 and C_2 are both large enough, the level of $3V_{in}$ can be output by the DC-DC converter section. In this case, if the switches S_1 and S_4 are turned ON and S_2 and S_3 being OFF, the bus voltage v_{bus} is equal to $3V_{in}$ as shown in Fig.3d. With similar method, the level of $-3V_{in}$ can be produced by turning switches S_1 and S_4 OFF, and S_2 and S_3 ON.

According the above analysis, the working states' combination of the seven-level version of the proposed inverter is concluded as shown in Tab.1. It can be seen from Tab.1 that there are eight working states for the inverter corresponding to seven voltage levels, including two zero level states. In each state, a maximum of only four switches are in conduction. And when the inverter operates alternatively in two adjacent states, there is only one or two switches' states needed to be changed.

TABLE I
Working states' combination of the seven-level inverter

No. of states	Bus voltage v_{bus}	Switching states						
		Q_0	Q_1	Q_2	S_1	S_2	S_3	S_4
1	$+3V_{in}$	0	1	1	1	0	0	1
2	$+2V_{in}$	0	1	0	1	0	0	1
3	$+V_{in}$	1	0	0	1	0	0	1
4	0	1	0	0	1	0	0	0
5		1	0	0	0	1	0	0
6	$-V_{in}$	1	0	0	0	1	1	0
7	$-2V_{in}$	0	1	0	0	1	1	0
8	$-3V_{in}$	0	1	1	0	1	1	0

3. Modulation Method

There are many modulation methods to control a multilevel inverter, such as classic carrier-based sinusoidal PWM (SPWM) method [6]. In this section, SPWM is also introduced to modulate the multilevel inverter, as follows. For the seven-level inverter, there are six carrier signals e_1~e_6 and a modulated sinusoidal signal e_S needed, as shown in Fig.4a which is the modulation logic circuit for the proposed seven-level inverter. Fig.4b shows the corresponding modulation waveforms, in which A_C is the

amplitude of the carrier signals. If defining the symbol A_S as the amplitude of the modulated sinusoidal signal, the modulation index M can be defined as

$$M = \frac{2A_S}{(N-1)A_C} \quad (1)$$

where N is the number of the levels and it is odd. For the proposed seven-level inverter, N=7.

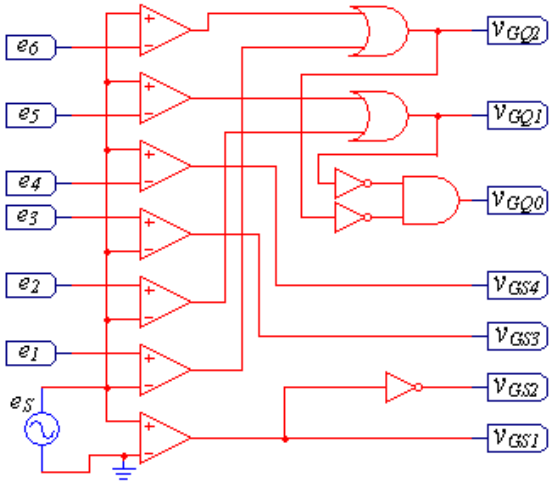

a. modulation logic circuit

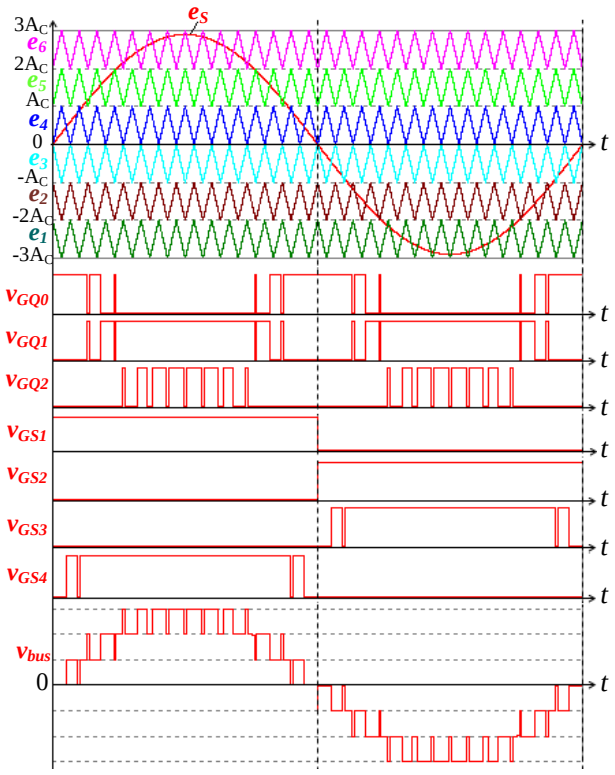

b. modulation waveforms

Fig.4: Modulation method for the proposed seven-level inverter

And the frequency modulation ratio can also be defined as

$$P = \omega_C / \omega_S \quad (2)$$

where ω_C and ω_S are the angular frequencies of the carrier signal and modulated signal respectively. And the desired output sinusoidal voltage therefore can be derived as (3).

$$v_O = \frac{N-1}{2} M V_{in} \sin \omega_S t \quad (3)$$

III. Gate Driver and Output Filter

1. Gate driver for the proposed inverter

For multilevel inverters, a large number of active switching elements are required and the drive circuit is needed for each switch. In this respect, the cost and complexity of the gate driver depends on the number of active switches required for the multilevel inverter. For the proposed inverter, although the number of active switches employed is much lesser than conventional multilevel inverter, its gate drive circuit is still a very important issue. Bootstrap capacitor driver (*BSCD*) is a mature gate drive technique and has traditionally been applied in various bridge circuits [7]. Based on the special structure of the proposed inverter, *BSCD* technique is also introduced to drive the all active switches.

In the proposed topology which consists of a full bridge and a multilevel DC-DC converter, the gate drivers for the full bridge is very simple and is not elaborated in the text. For the DC-DC conversion section, active switches Q_1 to Q_n are actually connected in series with Q_0 though diodes D_1' to D_n' respectively. And Q_0 can be turned ON just after all other switches Q_1 to Q_n being OFF. The voltage for the gate driver of Q_0 therefore can be supplied directly by the signal power V_{gate}. And the voltage sources for the gate drivers of Q_1 to Q_n could be implemented by using a bootstrap capacitor for each switch as shown in Fig.5. Take the diver circuit of Q_1, BSCD-1 as an example, when switch Q_0 is turned ON while Q_1 being OFF, the capacitor C_{B1} is charged by the signal power V_{gate} though D_{11}, D_1' and Q_0, the energy is stored in C_{B1} and its voltage is eventually equal to V_{gate}. When Q_0 is turned OFF, switch Q_1 could be controlled by its trigger signal v_{GQ1} and voltage as well as power are supplied by the capacitor C_{B1}. For other switches Q_i (i=2, 3, …, n), the gate drivers BSCD-i are totally the same as BSCD-1. The gate diver for the total inverter is therefore very simple and only one signal power V_{gate} is required.

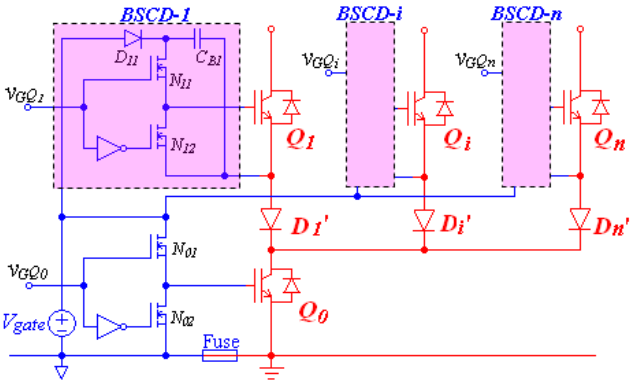

Fig.5: Gate driver for the proposed inverter

2. Output filter design for the proposed inverter

Comparing with 2-level inverter, the output performance of the multilevel inverters is more satisfactory in the terms of harmonics. The output filters therefore are easier to be designed. Usually, the multilevel inverters only need to employ an *LC* low-pass output filter with reasonable parameters to provide satisfactory output sinusoidal voltage. The detailed design methods of *LC* filter for PWM inverters have been introduced in [8], [9] and the technique is very mature, that is mainly based the considerations of reactive power and output voltage harmonics. Simply, the design steps of a *LC* filter for PWM inverters can be summarized as follows.

1). to determine the filter cut-off frequency ω_f referring to the carrier signals frequency ω_C and the modulated signal frequency ω_S, i.e.

$$\omega_f = \frac{1}{\sqrt{LC}} \tag{4}$$

and $$\omega_S < \omega_f < \omega_C \tag{5}$$

2). to determine the inductance of the filter according to the principle of minimum reactive power. For the pure resistance load, the reactive power Q_{LC} caused by the *LC* filter could be approximately expressed as

$$Q_{LC} \approx \omega_S I_O{}^2 L + \left(\frac{\omega_S}{\omega_f}^2 + \frac{\omega_S}{\omega_f}^4\right) U_O{}^2 \frac{1}{L} \tag{6}$$

where U_O and I_O are the rms values of the output voltage and load current respectively. The minimum reactive power is obtained when $\partial Q_{LC}/\partial L = 0$. The value of the inductor L therefore can be calculated by

$$L = \frac{U_O}{I_O \omega_f}\sqrt{1+\left(\frac{\omega_S}{\omega_f}\right)^2} \tag{7}$$

3). calculate the capacitance of the filter according the value of inductance *L* and the cut-off frequency ω_f, i.e.

$$C = \frac{1}{\omega_f{}^2 L} \tag{8}$$

IV. Simulation Experimental Verification

1. Simulation Results

To verify the feasibility of the proposed gate driver and the LC output filter developed for the multilevel inverter of Fig.1, a simulation model is built based on the seven-level topology, the multicarrier SPWM technique and the gate driver structure as shown in Figs. 2, 4a and 5 respectively. Fig.6 shows the simulated results and the simulation parameters are chosen as following: the dc input voltage V_{in} is 24V; the capacitances of C_1 and C_2 both are 1000μF; the carrier signals frequency and the modulated signal frequency are 40kHz and 400Hz respectively; the modulation index *M* is 0.96 and the load resistance is 22Ω; the signal power V_{gate} is 15V and the bootstrap capacitor is 1μF; the output filter inductance *L* and capacitance *C* are 850μH and 2.2μF respectively.

Simulation results indicate that the multilevel inverter is capable of generating a pure sinusoidal output voltage waveform v_O and this is benefited from the bootstrap gate driver circuit and the LC filter developed in this paper.

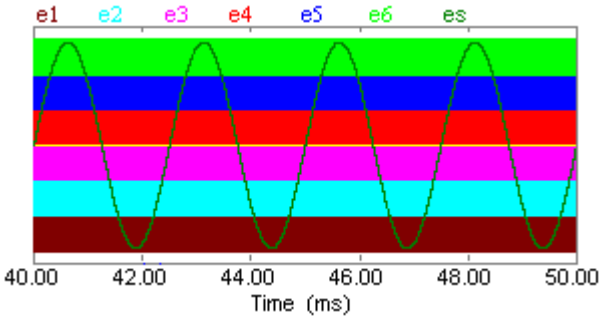

a. the carrier signals e_1~e_6 and the modulated signal e_S

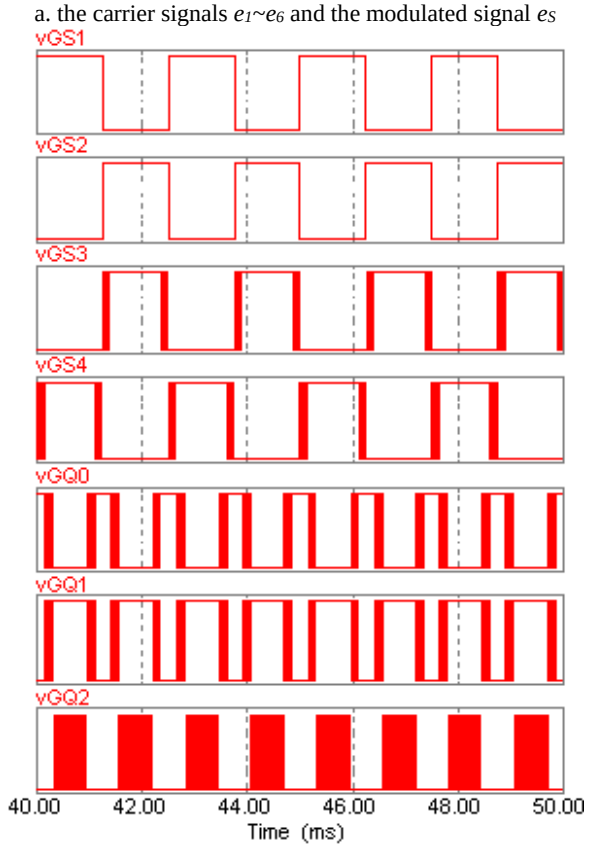

b. switching control signals

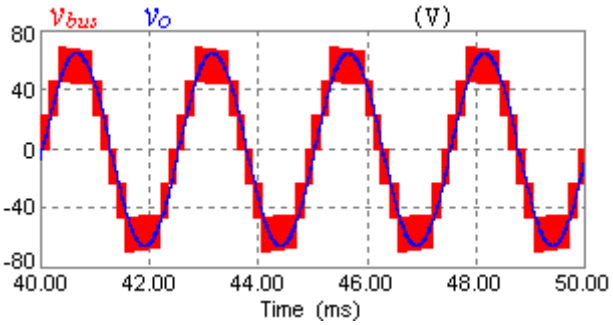

c. output voltage waveforms

Fig.6: Simulation results of the seven-level output

2. Experimental Results

A prototype of the seven-level version of the proposed inverter is developed to evaluate the performance of the proposed topology in the generation of a desired output

voltage waveform. The basic parameters are the same as that used for simulation and the switches are selected as following: S_1~S_4 and Q_0 are MOSFETs IRFB4019PBF; Q_1 and Q_2 are MOSFETs IRFI540A; MBR10100 are used as the diodes D_1, D_2 and D_{02}. The modulation index M is still 0.96. The experimental results are shown in Fig.7. As shown in Fig.7a, the output voltage waveforms are basically the same as the simulation results aforementioned except for the amplitude, which is slightly lower than the theoretical value the simulation result because the voltage drops of the switching devices. Fig.7b shows the frequency spectrum of the bus voltage v_{bus}. It can be seen that the lower order harmonics are small but the higher harmonics cannot be neglected, especially those closed to the carrier signals frequency. This issue is easily solved by the output LC filter as shown in Figs.7c and 7d, which show the frequency spectrum of the output voltage v_O.

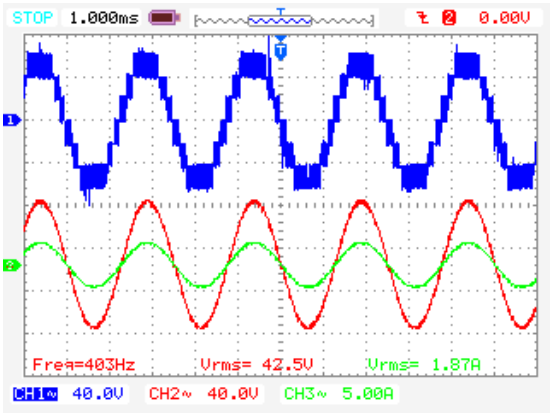

a. CH1: v_{bus}; CH2: v_O; CH3: i_O

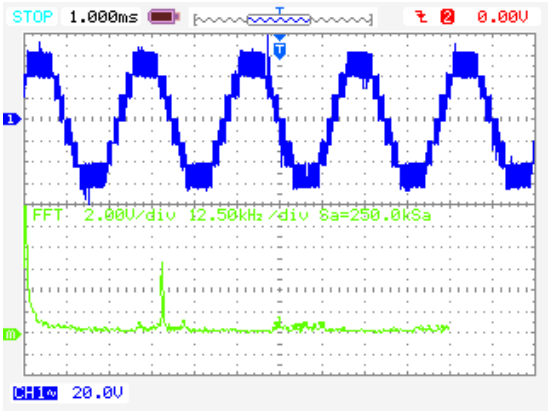

b. frequency spectrum of v_{bus} (0~125kHz)

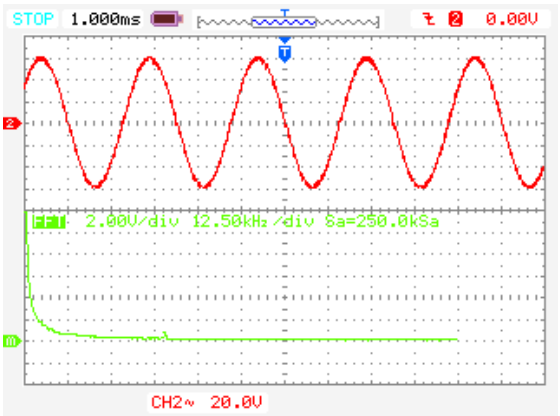

c. frequency spectrum of v_O (0~125kHz)

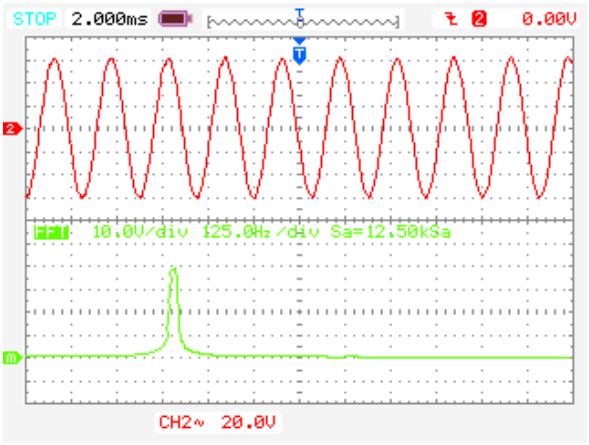

d. frequency spectrum of v_O (0~1.5kHz)

Fig.7: Experimental results of the seven-level inverter

IV. Conclusion

In this paper, a simple gate drive circuit and an output filter are developed for the multilevel inverter presented in [5]. With this bootstrap gate driver, only one voltage source is required to power the drive circuit of all switches employed in this inverter. This makes it has the advantages of small size and cost-effectiveness. With the LC filter, this inverter is capable of providing a pure sinusoidal output voltage waveform. And it is very suitable for aircraft APUs. Simulation and experimental results indicate the gate driver and the LC filter introduced in this paper provide a very well solution to promote the industrial applications of the multilevel inverter.

Acknowledgment

The authors grateful acknowledge the financial support of Innovation and Technology Fund of Hong Kong ITC and JL Ecopro Tech. Ltd under the project number UIM245.

References

[1] J. Rodriguez, J. S. Lai, and F. Z. Peng, "Multilevel inverters: Asurvey of topologies, control, and applications", *IEEE Transaction on Industrial Electronics*, vol.49, no.4, pp.724–738, Dec. 2002.

[2] J. Rodriguez, S. Bernet, P.K. Steimer, and I.E. Lizama, "A survey on neutral-point-clamped inverters," *IEEE Transaction on Industrial Electronics*, vol.57, no.7, pp.2219–2230, Jul. 2010.

[3] M. F. Escalante, J. -C. Vannier and A. Arzande, "Flying capacitor multilevel inverters and DTC motor drive applications," *IEEE Trans. Ind. Electron.*, vol. 49, no. 4, pp. 809–815, Aug. 2002.

[4] M. Malinowski, K. Gopakumar, J. Rodriguez, M. A. Pérez, "A Survey on Cascaded Multilevel Inverters," *IEEE Trans. Ind. Electron.*, vol. 57, no. 7, pp. 2197–2206, Jul. 2010.

[5] Yuanmao Ye, K.W.E. Cheng, Junfeng Liu, and Kai Ding, "A Step-Up Switched-Capacitor Multilevel Inverter with Self Voltage Balancing," *IEEE Trans. Ind. Electron.*, vol. 61, no. 12, pp. 6672-6680, Dec. 2014.

[6] Mwinyiwiwa B., Wolanski Z., Yiqiang Chen, Boon-Teck Ooi, "Multimodular multilevel converters with input/output linearity," *IEEE Transactions on Industry Applications*, vol.33, no.5, pp.1214-1219, Sep./Oct. 1997.

[7] Graczkowski J.J., Neff K.L., Kou X., "A Low-Cost Gate Driver Design Using Bootstrap Capacitors for Multilevel MOSFET Inverters", *CES/IEEE 5th International Power Electronics and Motion Control Conference*, Aug. 2006.

[8] Soo-Hong Kim, Yoon-Ho Kim, Kang-Moon Seo, Sang-Seok Bang, Kwang-Seob Kim, "Harmonic analysis and output filter design of NPC multi-level inverters", *37th IEEE Power Electronics Specialists Conference*, June 2006.

[9] Hyosung Kim and Seung-Ki Sul, "A Novel Filter Design for Output LC Filters of PWM Inverters", *Journal of Power Electronics*, vol.11, no.1, pp.74-81, Jan. 2011.

Soft-switching Topologies for Switched Reluctance Motors in the Application of Electric Vehicles

Jingwei Zhu[1] K.W.E Cheng[2] N.C. Cheung[3]

[1,2,3] Power Electronics Research Centre, Department of Electrical Engineering, The Hong Kong Polytechnic University, Hong Kong
E-mail: 15901658r@connect.polyu.hk, eeecheng@polyu.edu.hk, norbert.cheung@polyu.edu.hk

Abstract- two topologies of soft-switching for the switched reluctance motor (SRM) are proposed in this paper to reduce the switching loss and EMI in the chopping and commuting periods. The design circuit of the topologies are shown and the feature of the current or voltage of resonant elements are analyzed in theory and confirmed by simulation of Matlab/Simulink. Besides, the energy loss of the soft-switching circuit for the second topology is calculated and compared with the conventional one. The loss is computed under different rotating speeds to simulate electrical vehicle (EV) running under various speeds and the advantage of the proposed circuit is proved.

Keywords-SRM, Matlab/Simulink, soft-switching, energy loss, topology

I. INTRODUCTION

With the increasingly serious environment pollution and energy crisis, EV has become a new trend for future industrial vehicle study due to its high efficiency and low emission. Motor drive is the central part of EV because of offering enough power for its performing. The SRM has the advantage over other kinds of motors as it has a simple structure, low cost, high efficiency, easy control, low starting current and high pull-up torque. Therefore, it has a potential prospect in the application of machine drives of EV. But in order to optimize a control strategy for SRM drive, high frequency is required for accurate current and flux linkage regulation, causing considerable switching losses and EMI. Soft switching technology is an efficient method in lowering these losses for EV in normal urban driving [1].

In [2], resonant DC link (RDCL) is utilized to achieve ZVS on and ZCS off, but the resonant inductor is in series with the inverter-bridge leading to unnecessary loss since both resonant and load current flow through this resonant inductor. Literature [3] introduces additional inductors and capacitors into the topology, however, there's a resonant inductor in the main loop as well. A novel topology is put forward in [4] with PWM method to reduce the switching losses, but the resonant inductor is still in the main circuit. The soft-switching topology in [5] can only attain ZVS on for phase switches. Document [6-8] solved the inverter problems above, but when there is no load, the formation of zero voltage between the DC bus encounters great difficulties.

This paper proposes two topologies to reduce the switching losses and settle the challenges above. The topology in section II utilizes only one auxiliary switch and remains the resonant inductor in the resonant circuit, thus declining the current flowing through it greatly. Besides, the number of the auxiliary elements is reduced to a great extent. Section III gives an improved topology to achieve controlling the zero voltage duration freely and no current flowing through the resonant inductor during normal conducting time, although it adds two additonal auxiliary switches. Section IV makes a comparison of the energy losses between the improved topology in section III and the convential one; furthermore, some analysis is offered.

II. A SUITABLE SOFT-SWITCHING TOPOLOGY FOR THE SRM

The designed circuit is in the following Figure 1:

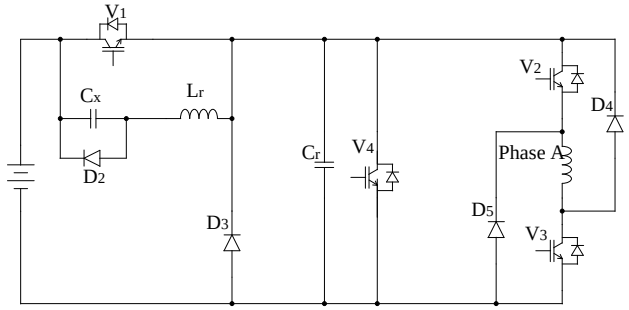

Figure 1. Schematic of the new soft-switching topology.

In this Figure 1, one phase of the SRM is simplified as a constant inductance during the soft-switching period since it is short enough. And the parameter of the elements in the circuit is in the following Table 1:

Table 1: Circuit Parameters for the Topology

E (V)	300	C_s (pF)	0.1
C_x (nF)	1000	L_r (μF)	60
C_r (nF)	30	L_A (mF)	10

V_1, V_2, V_3, V_4 of the switching components are all selected as IGBT. This proposed circuit can simplify the control of switching elements, reduce the number of switching and resonant components to lower the hardware cost. Besides, it has extra advantages of each switch turning on-off at zero voltage and the maximum enduring voltage is equal to that of the DC source. Meanwhile, because of no series voltage-divider capacitors between the DC bus, there's no potential variation of the neutral point [9].

The theoretical waveforms of the switching signal, voltage or current of the resonant components are shown as follows in Figure 2:

This circuit can be divided into six working modes

Mode I ($0\sim t_0$): it's the initial condition of the whole circuit with V_1, V_2, V_3 on and V_4 off. The circuit is stable and there is a constant reverse current I_{L0} flowing through the resonant inductor L_r.

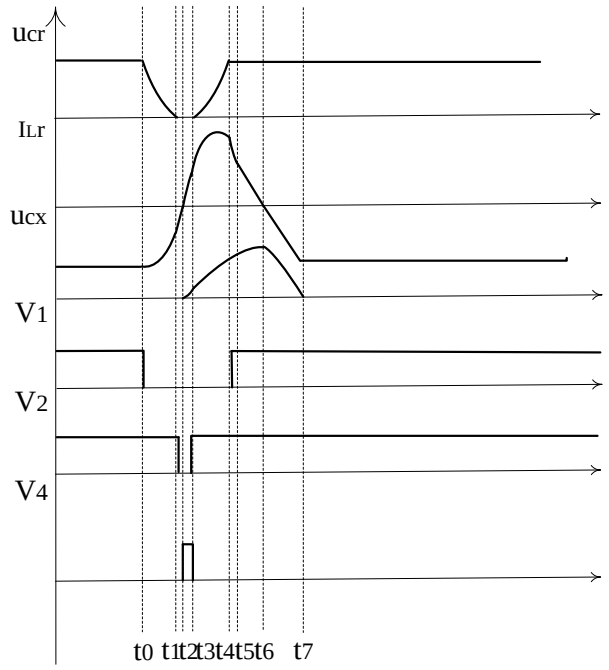

Figure 2. theoretical waveform for the novel topology

Mode II (t_0~t_1): when V_1 is off, L_r and C_r begin their resonance with both the current I_{lr} and voltage u_{cr} decreasing. The energy of L_r feeds back to the battery while that of C_r is transferred to both the winding and the battery. With C_r discharging, the DC bus voltage is declining gradually until zero. The differential equation is as follows:

$$u_{cr} = -L_r \cdot \frac{di_r}{dt} + E \tag{1}$$

$$C_r \cdot \frac{du_r}{dt} = i_r - I_0 \tag{2}$$

Then, with the initial value $u_{cr}(t_0) = E$, $i_{cr}(t_0) = -I_{L0}$, we can get

$$u_{cr} = E - \frac{(I_0 + I_{L0})}{\omega_r C_r} \sin[\omega_r (t - t_0)] \tag{3}$$

$$i_r = I_0 - (I_0 + I_{L0}) \cos[\omega_r (t - t_0)] \tag{4}$$

where, $\omega_r = \frac{1}{\sqrt{L_r C_r}}$, I_0 is the current of the winding load. Therefore, the mode II time,

$$T_2 = \frac{1}{\omega_r} arcsin \frac{\omega_r C_r E}{I_0 + I_{L0}} \tag{5}$$

Mode III (t_1~t_2): when u_{cr} reaches zero, diode D_3 conducts which clamps the DC bus voltage at zero and V_2 can be switched off at zero voltage. During this period, L_r bears a constant voltage of the DC source and i_r decreases linearly until it reaches zero point. So,

$$i_r = \frac{E}{L_r}(t - t_1) - I_1 \tag{6}$$

Thus, the mode III time,

$$T_3 = \frac{L_r I_1}{E} \tag{7}$$

Mode IV (t_2~t_3): IGBT V_4 is turned on to keep i_r positive and the capacitor u_{cx} is conducting. So C_x and L_r start their resonance under the DC bus voltage until it i_r attains its setting value I_2 at the moment t_3. At the end of this period, the switch V_2 is turned on at zero voltage point of the DC bus. Then IGBT V_4 is turned off. We can get the equation,

$$u_{Cx} + L_r \frac{di_r}{dt} = E \tag{8}$$

$$C_x \frac{du_{Cx}}{dt} = i_r \tag{9}$$

From (8) and (9), the result is

$$u_{Cx} = E - E\cos[\omega_x (t - t_2)] \tag{10}$$

$$i_r = \omega_x C_x E \sin[\omega_x (t - t_2)] \tag{11}$$

Therefore, the duration of this mode is

$$T_4 = \frac{1}{\omega_x} \arcsin\left(\frac{I_2}{C_x \omega_x E}\right) \tag{12}$$

Mode V(t_3~t_4): With V_4 switched off, L_r, C_x, C_r begin their resonance together. Because of $C_x >> C_r$, the series capacitor can be simplified as

$$\frac{C_x C_r}{C_x + C_r} \approx C_r \tag{13}$$

In this mode, u_{Cx} can be regarded as constant U. During the resonance process, both L_r and C_r are charged, with i_r and u_{Cr} increasing till u_{Cr} getting to the DC bus voltage.
The differential equations are as follows:

$$E - U = L_r \frac{di_r}{dt} + u_{cr} \tag{14}$$

$$i_r - I_0 = C_r \frac{du_{cr}}{dt} \tag{15}$$

Then we can calculate,

$$u_{cr} = (E - U)(1 - \cos[\omega_r (t - t_3)]) + \frac{I_2 - I_0}{\omega_r C_r} \sin[\omega_r (t - t_3)] \tag{16}$$

$$i_r = I_0 + (I_2 - I_0)\cos[\omega_r (t - t_3)] + \omega_r C_r (E - U) \sin[\omega_r (t - t_3)] \tag{17}$$

From the outcome, when u_{cr} increases to $(E - U)$, i_r reaches its maximum and from then on, u_{cr} augments while i_r decreases. The duration of this mode can be calculated as

$$T_5 = \frac{1}{\omega_r} \left(\arcsin\left(\frac{E - U}{M}\right) + \arcsin\left(\frac{U}{M}\right)\right) \tag{18}$$

where, $M = \sqrt{\frac{(I_2 - I_0)^2}{\omega_r^2 C_r^2} + (E - U)^2}$

Mode VI(t_4~t_7): During this mode, two parts of it need to be analysed. To start with, when i_r is still positive, C_x and L_r start resonance with u_{cx} increasing and i_r declining. Before i_r descends to the winding load current I_0, Diode

D1 is conducting during which time the switch V_1 can be turned on under zero voltage condition. The first part ends with u_{cx} arriving at its peak and i_r dropping to zero. The second part begins when i_r is negative, during which, C_x is discharged and i_r increases reversely. It comes to an end when u_{cx} drops to zero voltage and Diode D_2 is on. Later, it comes back to Mode I and start a new circulation.
The equation is as follows:

$$u_{cx} + L_r \frac{di_r}{dt} = 0 \tag{19}$$

$$C_x \cdot \frac{du_{cx}}{dt} = i_r \tag{20}$$

Then the value we get is

$$u_{cx} = Ucos[\omega_r(t - t_4)] + \frac{I_3}{C_x\omega_x} sin[\omega_r(t - t_4)] \tag{21}$$

$$i_r = I_3 \cos[\omega_r(t - t_4)] - C_x\omega_x Usin[\omega_r(t - t_4)] \tag{22}$$

The length of time is

$$T_6 = \frac{1}{\omega_x}(\pi - arctan\frac{UC_x\omega_x}{I_3}) \tag{23}$$

According to the theory analysis above, a simulation of one circulation based on Matlab/Simulink has been done to confirm the theory. The switching signal is applied on the basis of the calculated duration of six modes. The initial current I_{l0} is set as -30A, I_2 is selected as 37.6A and winding load current I_0 is chosen as 12A.

The waveform figure is shown in the following Figure 3:

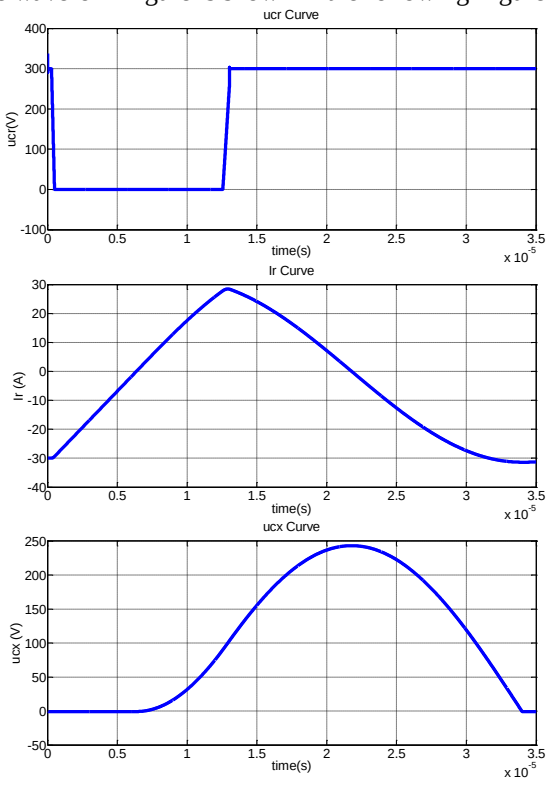

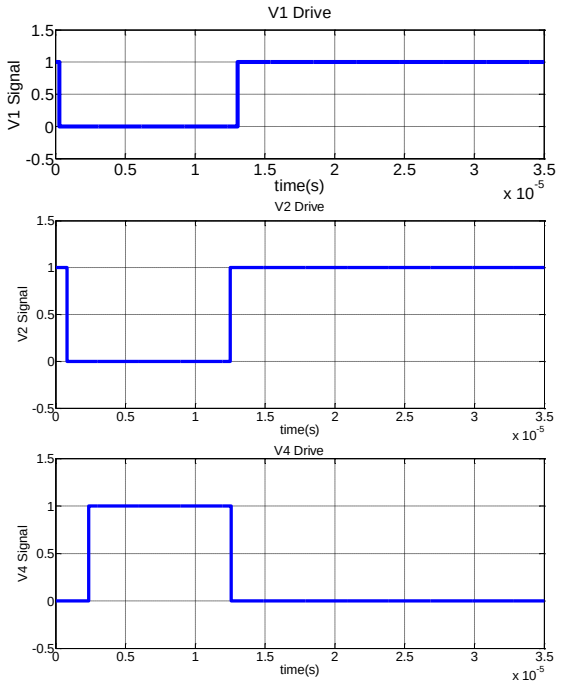

Figure 3. Waveform from Matlab/Simulink

The simulation results agree with the theoretical analysis, confirming the validity of this new topology.

III. An Improved Topology For The SRM

The proposed topology is shown below in Figure 4:

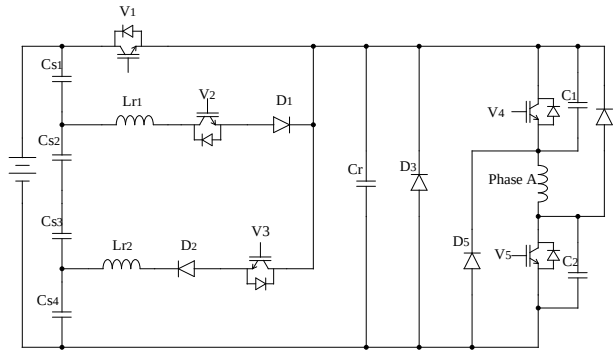

Figure 4. Schematic of the improved soft-switching topology

In this Figure 4, one phase of the SRM is also simplified as a constant inductance during the soft-switching period since it is short enough. And the parameter of the elements in the circuit is in the following Table 2:

Table 2: Circuit Parameters for the Improved Topology

$E(V)$	240	$L_A(mH)$	0.01
$C_r(nF)$	25	$L_r(\mu H)$	10
$C_i(pF)$ $(i$ from 1 to 2$)$	0.1	$L_{r1}(\mu H)$	10
C_{si} (μF) $(i$ from 1 to 4$)$		25	

V_1, V_2, V_3, V_4, V_5 are all IGBT in the schematic. This improved circuit has the advantage of controlling the zero voltage time by selecting the turning-on time of V_2 [10]. And the theoretical waveforms of the elements in this topology are shown as follows in Figure 5:

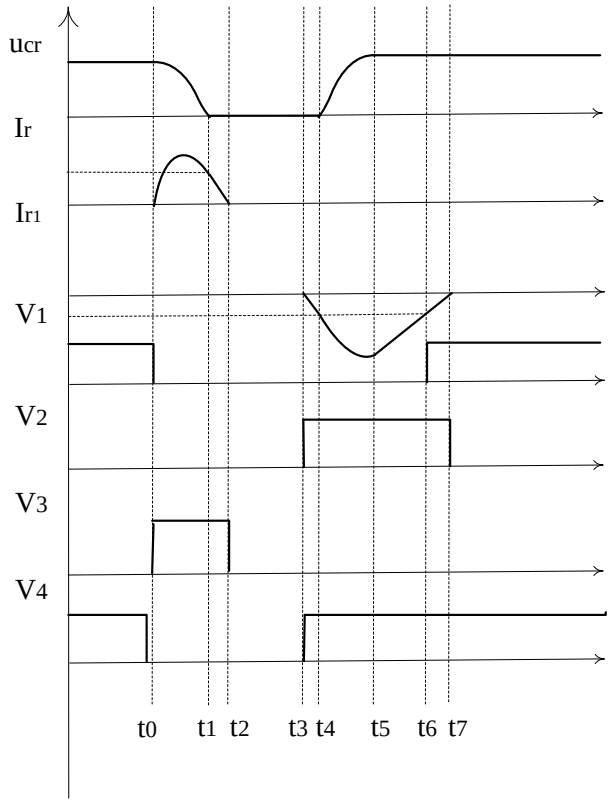

Figure 5. theoretical waveforms for the improved topology

This topology can be separated into eight modes.

Mode I ($0\sim t_0$): both V_2 and V_3 are off while V_1, V_4, V_5 are on during this period. Phase A is conducting.

Mode II ($t_0\sim t_1$): At the moment t_0, the switch V_1, V_2 and V_4 are all been turned off with only V_3 and V_5 on. Because of the existence of C_i, V_4 is turned off at zero voltage. Meanwhile, V_1 is also turned on during zero voltage stage. C_r, V_3, L_r, C_4 makes up a loop with C_r and L_r starting their resonance. Because of no sudden change of current in L_r, V_3 is switched on under a zero current condition. At the beginning, C_r is discharged while i_r increases until u_{cr} reaches $\frac{E}{4}$, then i_r starts to decrease ending with u_{cr} getting to the zero voltage point. At the time t_1, C_r is clamped by D_3 to keep a constant zero voltage situation. The equations of it are as follows:

$$u_{cr} = L_r \cdot \frac{di_r}{dt} + \frac{E}{4} \tag{23}$$

$$C_r \frac{du_{cr}}{dt} = -i_r \tag{24}$$

The results are calculated as

$$u_{cr} = \frac{E}{4} + \frac{3}{4}Ecos[\omega_r(t-t_0)] \tag{25}$$

$$i_r = \frac{3}{4}E\omega_r C_r sin[\omega_r(t-t_0)] \tag{26}$$

Therefore, we can get the duration of this period

$$T_2 = \sqrt{L_r C_r}\arccos(-\frac{1}{3}) \tag{27}$$

Mode III ($t_1\sim t_2$): since C_r is clamped by D_3, L_r will begin to discharge under the reverse voltage $\frac{E}{4}$ until it arrives at zero point.

$$i_r = I_1 - \frac{E(t-t_1)}{4L_r} \tag{28}$$

The time period is

$$T_3 = \frac{4L_r I_1}{E} \tag{29}$$

Mode IV ($t_2\sim t_3$): during this mode, no switches are on and the length of period can be controlled by deciding the turning on moment of V_2. V_3 is both zero voltage and zero current turned off. Therefore, the switching on moment of V_4 can be located during the zero voltage stage definitely without thinking about the value of L_r and C_r.

Mode V ($t_3\sim t_4$): V_2, V_4 and V_5 are on while V_1 and V_3 are off. The phase winding is conducting. Because the DC bus voltage is zero, V_4 is ZVS on and V_2 is ZCS on as a result of the existence of L_{r1}. During this mode, u_{cr} still keeps zero voltage and i_r increases reversely under the voltage of $\frac{3}{4}E$ until it reaches the winding current I_0.

$$i_{r1} = -\frac{3E}{4L_{r1}}(t-t_3) \tag{30}$$

Therefore, the length of this period is

$$T_5 = \frac{4L_{r1}I_0}{3E} \tag{31}$$

Mode VI ($t_4\sim t_5$): C_r and L_{r1} start their resonance and it lasts until u_{cr} reaches E.

$$\frac{3}{4}E = -L_{r1}\frac{di_{r1}}{dt} + u_{cr} \tag{32}$$

$$C_r \frac{du_{cr}}{dt} = -i_{r1} - I_0 \tag{33}$$

Then we can get the result

$$u_{cr} = \frac{3}{4}E - \frac{3}{4}Ecos[\omega_r(t-t_4)] \tag{34}$$

$$i_{r1} = -I_0 - \frac{3}{4}EC_r\omega_r \sin[\omega_r(t-t_4)] \tag{35}$$

$$T_6 = \frac{1}{\omega_r}\arccos\left(-\frac{1}{3}\right) \tag{36}$$

Mode VII ($t_5\sim t_6$): Since during this mode, $|i_{r1}|>I_0$, the voltage of $\frac{E}{4}$ is added to L_{r1}. C_{si}, V_1, V_2, L_{r1} form a series loop. V_1 is clamped by the diode, so it's ZVS on during this period.

$$i_{r1} = -I_0 - \frac{\sqrt{2}}{2}EC_r\omega_r + \frac{E}{4L_{r1}}(t-t_5) \tag{37}$$

So the duration is

$$T_7 = 2\sqrt{2}\omega_r C_r L_{r1} \tag{38}$$

Mode VIII $(t_6 \sim t_7)$: L_{r1} is still under $\frac{E}{4}$ voltage and the changing rule of i_{r1} is the same as that in Mode VII. When i_{r1} reaches zero, V_2 is ZCS off. Then a new circulation begins.

$$T_8 = \frac{4L_{r1}I_0}{E} \tag{39}$$

The simulation results during one time period of this topology is shown as follows in Figure 6:

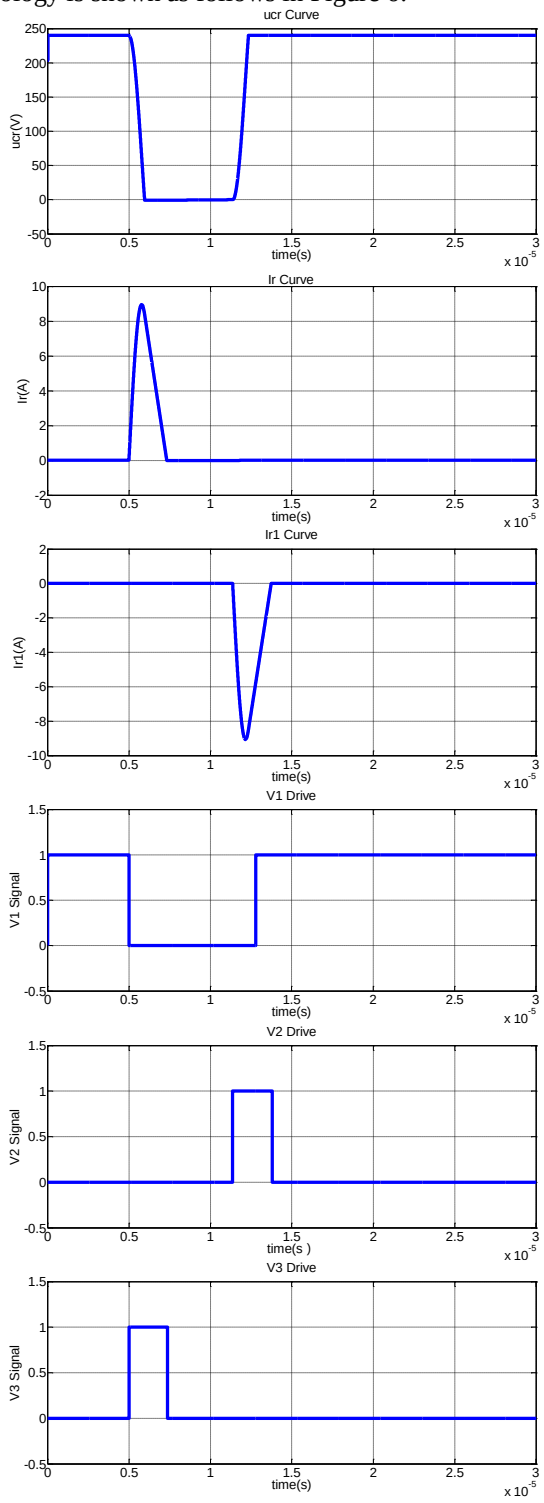

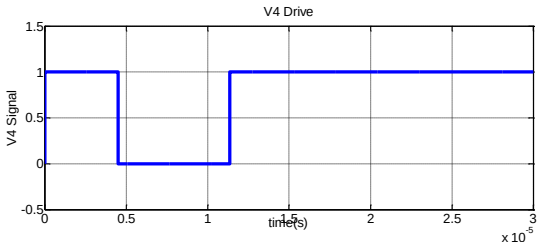

Figure 6. Waveforms from Matlab/Simulink of the improved topology

Then the improved topology is added into a whole current chopping control (CCC) system for a 6/4 SRM. And the DC source voltage is changed to 120V with other parameters unchanged. CCC is a common control method for SRM. When a SRM is running at a low speed, it has a small rotating EMF and a high value of di/dt. Also, because of long period for inductance increasing, we usually utilize CCC to prevent overcurrent in each phase. It regulates the upper and lower limit of the permitted current and keep θ_{on}、θ_{off} constant, in order to limit the value of current within an expected range. Its principle is in the following shown in Figure 7:

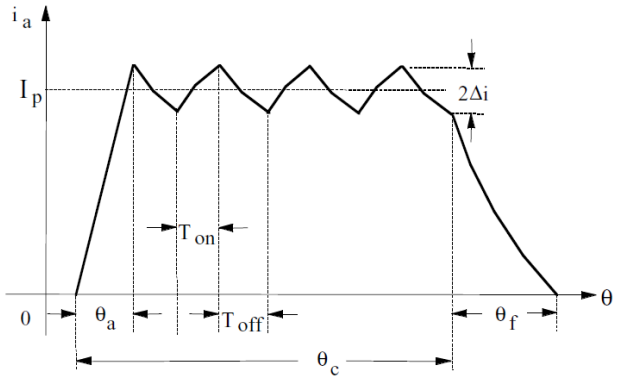

Figure 7. I_p is the chopping current of the winding with the upper limitation $I_p + \Delta i$ and the lower limitation $I_p - \Delta i$

The simulation results of the waveforms on the basis of Matlab/Simulink are as follows in Figure 8:

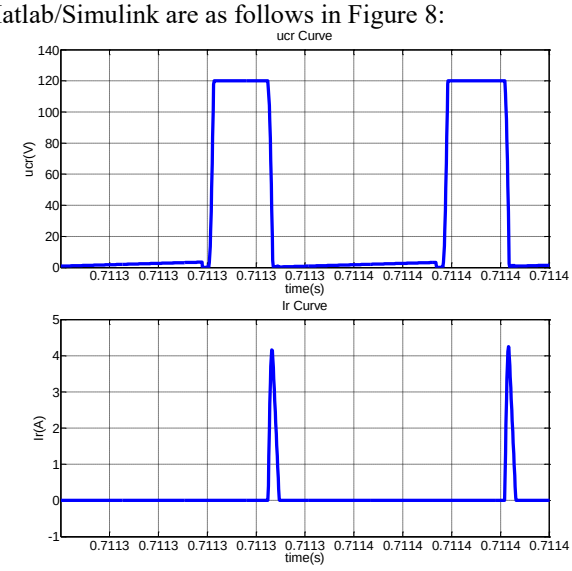

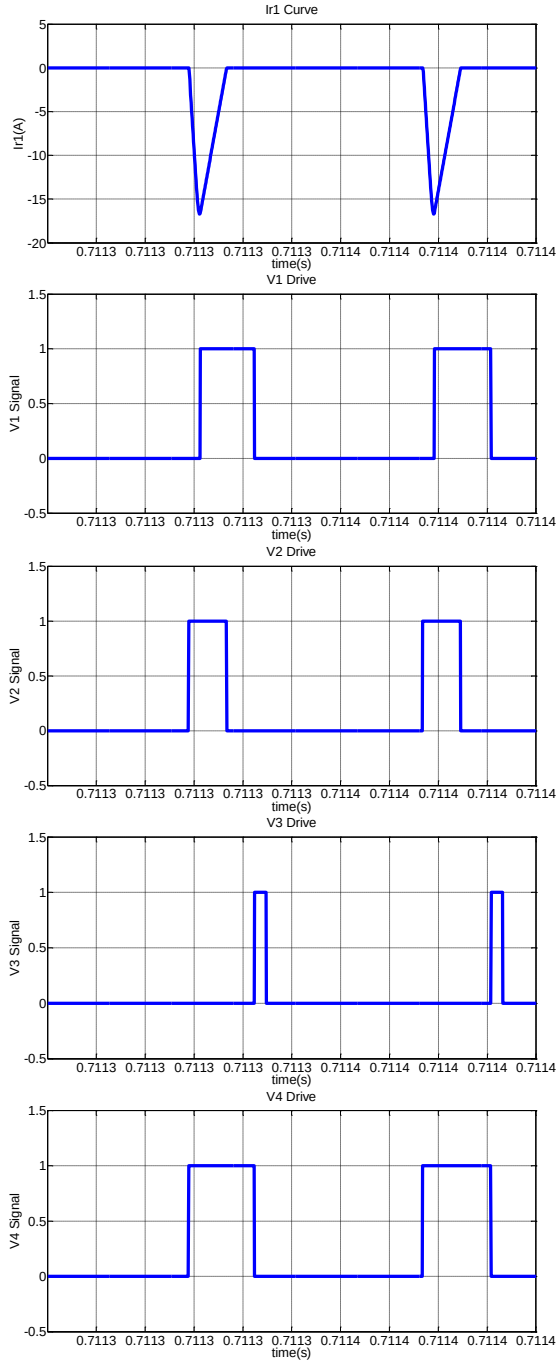

Figure 8. Waveform from Matlab/Simulink of the improved topology when applied to a CCC system for a 6/4 SRM

IV. Comparison Of The Improved Soft-switching Topology With The Conventional One In The Applications Of Electric Vehicles

According to the analysis of the mode of the improved topology, all the switching elements achieve the ZVS or ZCS on-off, so the switching loss is zero. However, because of increasing the number of auxiliary switches and diodes, the conducting loss will rise. It is known that the losses include the sorts of switching and conducting. Therefore, a comparison of loss between the proposed improved topology and the traditional one is needed.

The additional conducting losses come from the clamped diode of V_1, diodes D_1, D_2, D_3 and IGBT V_1, V_2, V_3. f_0 in the following equations is the switching frequency of current chopping control.

$$P_D = f_0 U_{ce} \int_0^{T_7} (-\frac{\sqrt{2}}{2} E C_r \omega_r + \frac{E}{4L_{r1}} t) dt \quad (40)$$

$$P_{D3} = f_0 U_{ce} \int_0^{T_3} (I_1 - \frac{Et}{4L_r}) dt \quad (41)$$

$$P_{D2} = f_0 U_{ce} (\int_0^{T_2} \frac{3}{4} E \omega_r C_r \sin(\omega_r t) dt + \int_0^{T_3} (I_1 - \frac{Et}{4L_r}) dt) \quad (42)$$

$$P_{D1} = f_0 U_{ce} [\int_0^{T_5} \left(-\frac{3E}{4L_{r1}} t\right) dt + \int_0^{T_6} \left(-I_0 - \frac{3}{4} E C_r \omega_r \sin(\omega_r t)\right) dt + \int_0^{T_7} \left(-I_0 - \frac{\sqrt{2}}{2} E C_r \omega_r + \frac{E}{4L_{r1}} t\right) dt + \int_0^{T_8} (-I_0 + \frac{E}{4L_{r1}} t) dt] \quad (43)$$

$$P_{V_1} = I_0^2 R T_1 + \int_0^{T_8} (\frac{E}{4L_{r1}} t)^2 R dt \quad (44)$$

$$P_{V_2} = \int_0^{T_5} (\frac{3E}{4L_{r1}} t)^2 R dt + \int_0^{T_6} [-I_0 - \frac{3}{4} E C_r \omega_r \sin(\omega_r t)]^2 R dt + \int_0^{T_7} \left(-I_0 - \frac{\sqrt{2}}{2} E C_r \omega_r + \frac{E}{4L_{r1}} t\right)^2 R dt + \int_0^{T_8} (-I_0 + \frac{E}{4L_{r1}} t)^2 R dt \quad (45)$$

$$P_{V_3} = \int_0^{T_2} [\frac{3}{4} E \omega_r C_r \sin(\omega_r t)]^2 R dt + \int_0^{T_3} (I_1 - \frac{Et}{4L_r})^2 R dt \quad (46)$$

Where D is the clamped diode of V_1, U_{ce} is the forward voltage drop of a diode.

For the hard switching period in a conventional topology for the SRM, the switching process of the voltage and current can be simplified as the following equation as:

$$u_{ce} = E - \frac{E}{\Delta t} t \quad (47)$$

$$i_{ce} = \frac{I_0}{\Delta t} t \quad (48)$$

$$P_{sw} = \frac{1}{T_0} \int_0^{T_0} u_{ce} \cdot i_{ce} dt = \frac{2}{T_0} \int_0^{\Delta t} u_{ce} \cdot i_{ce} dt = \frac{1}{3} E I_0 f_0 \Delta t \quad (49)$$

Where, the switching period T_0 is 4×10^{-5}s, voltage rising and current descending time Δt is 2×10^{-7}s.

In Table 3, power loss of both topologies is shown as below:

Table 3: Power Loss Of The Conventional And Improved Topology

n(r/min)	Conventional		Soft-switching		Percentage saved(%)
	I_0(A)	P	I_0(A)	P	
100	9.0	1.80	8.80	1.19	33.9
200	9.8	1.96	9.60	1.30	33.7
300	10.6	2.12	10.4	1.41	33.5
400	11.3	2.26	11.1	1.51	33.2
500	12.0	2.40	11.8	1.60	33.3
600	12.6	2.52	12.3	1.67	33.7
700	13.3	2.66	13.0	1.77	33.5
800	13.8	2.76	13.5	1.84	33.3
900	14.3	2.86	14.0	1.91	33.2

1000	14.8	2.96	14.5	1.98	33.1

The comparison curve of both topologies for the power loss is shown in the following Figure 9:

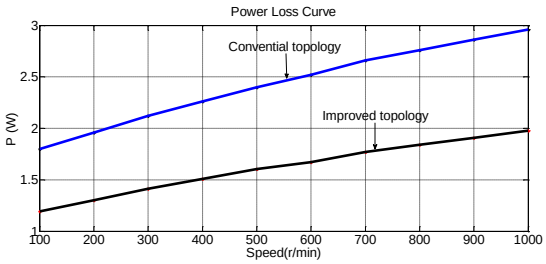

Figure 9. comparison of power loss for different topologies under various speed

From the comparison between these two topologies, less power loss of the proposed topology is seen in the table and figure, about 33 percent of energy saving. Furthermore, with the vehicle speed increasing, the current produced by the DC source ascends, thus increasing the energy or power loss.

VI. Conclusion

This paper proposes two topologies of soft-switching for the SRM drive. Each topology is analysed theoretically and calculated by equations to gain the ideal waveforms of the auxiliary components in the soft-switching part. These topologies also have their own deficiencies. The first one has current flowing through the resonant inductance during normal conducting time increasing extra loss and the zero voltage period can't be controlled. Furthermore, the auxiliary switching element is in the main circuit. As for the second improved topology, it solved most of the problems of the former one except one switching device in the main loop by adding another two assistant switching components. The waveforms of the above two topologies are confirmed by simulation based on Matlab/Simulink. Besides, the second improved topology is applied to the CCC system of a 6/4 SRM to prove that power loss of the proposed one is much less than the traditional one under various running speed for EV. Therefore, the proposed topologies has their potential prospects in the application of EV motor drives.

Reference

[1] Mehrdad Ehsani, Khwaja M. Rahman, Maria D. Bellar, Alex J. Severinsky, "Evaluation of Soft Switching for EV and HEV Motor Drives",IEEE Transactions on Industrial Electronics, Vol. 48, No. 1, February 2001

[2] Luo Jianwu, Zhan Qionghua, Deng Qiong, "Study of a Novel Soft-switching Converter for Switched Reluctance Motor [J]". Proceedings of the CSEE, 2005, 25 (17): 142-149

[3] J. Shukla, B.G. Fernandes, "Three-phase soft-switched PWM inverter for motor drive application", Electric Power Applications, IET, 2007: 93-104

[4] Luo Jianwu, Qionghua Zhan, "A Novel Soft-Switching Converter for Switched Reluctance Motor:Analysis, Design and Experimental Results", Electric Machines and Drives, 2005 IEEE International Conference, pages: 1955-1961

[5] Murai Y, Cheng J, Sugimoto S, Yoshida, M, " A Capacitor-boosted Soft-switched Switched Reluctance Motor Drive [C]", Proceedings of Applied Power Electronics Conference and Exposition. Piscataway: IEEE Inc, 1999: 424-429.

[6] Ming Zhengfeng, Zhong Yanru, Ning Yaobin, "A Novel Transition DC-rail Parallel Resonant Zero Voltage Three Phase PWM Voltage Source Inverter", Transactions of China Electrotechnical Society, 2001, 16(6): 31-35.

[7] Chen Guocheng, Sun Chengbo, Zhang Linglan, "The Analysis of a Novel ZVS Resonant DC-link Inverter Topology", Transactions of China Electrotechnical Society,2001, 16(4): 50-55

[8] Pan Zhiyang, Luo Fanglin, "Novel Soft Switching Inverter for Brushless DC Motor Variable Speed Drive System", IEEE Transactions on Power Electronics, 2004, 19(2): 280-288.

[9] Wang Qiang, Wang Tianshi, " A Parallel Resonant DC Link Inverter Applied to Motor Drives", Electric Machines And Control, 2013, Vol.17, No.1.

[10] Yang Jinling,Zhang Yingjun,Xie Binhong, "A new SRM soft switching power circuit", Journal of China Coal Society,2014,39(1):179-185

Biographies

Jingwei Zhu received his B.S. degree in 2015 in Electrical Engineering & Automation from Zhejiang University, Hangzhou, China.
He joined the department of Electrical Engineering, The Hong Kong Polytechnic University as a postgraduate. His main research interests are in the field of power electronics and motor drives.

K.W.E.Cheng obtained his BSc and PhD degrees both from the University of Bath in 1987 and 1990 respectively. Before he joined the Hong Kong Polytechnic University in 1997, he was with Lucas Aerospace, United Kingdom as a Principal Engineer.
He received the IEE Sebastian Z De Ferranti Premium Award (1995), outstanding consultancy award (2000), Faculty Merit award for best teaching (2003) from the University and Silver award of the 16th National Exhibition of Inventions. Faculty Engineering Industrial and Engineering Services Grant Achievement Award (2006), Brussels Innova Energy Gold medal with Mention (2007), Consumer Product Design Award (2008), Electric vehicle team merit award of the Faculty (2009), Special Prize and Silver Medal of Geneva's Invention Expo (2011) and Eco Star award (2012). He has published over 250 papers and 7 books. He is now the professor and director of Power Electronics Research Centre.

Ideas for Future Electric Aircraft System

S. Raghu Raman K. W. Eric Cheng N.C. Cheung

Power Electronics Research Centre, Department of Electrical Engineering, The Hong Kong Polytechnic University, Hong Kong
E-mail: raghu.raman.1990@ieee.org

Abstract – This design paper proposes few improvements on the existing electrical network in the aircraft system. It also suggests improvement in the starter circuitry by introducing super capacitors to reduce the number of batteries onboard to ensure improved safety and reliability. It proposes higher frequency of power distribution owing to several benefits. There are several advantages of high frequency AC power distribution over conventional DC distribution and low frequency AC power distribution. This paper explores the idea of employing switched capacitor and switched inductor converters to design multi-level inverters for high frequency AC power supplies for power distribution.

Keywords – Electric Aircraft, Multi – level inverters, Switched – Capacitor, Switched – Inductor.

I. INTRODUCTION

High frequency AC (HFAC) power distribution systems (PDS) have been popular since the 1980s when NASA proposed a 20 kHz, 440 V_{rms}, for their space station [1] & [2]. Since then HFAC PDS has emerged as a popular research area and has had several applications utilizing it. HFAC PDSs find application in telecommunication, renewable based micro-grid and computer power supply, aerospace and lighting systems. A comprehensive review on HFAC systems has been done in [3].

Basic power distribution architecture of HFAC PDS and DC PDS is clearly shown in Fig. 1 and Fig. 2. HFAC PDSs offer several benefits in comparison to conventional DC distribution systems. They include –

- Cost reduction due to reduction in the number of power conversion stages.
- Overall improved efficiency
- DC PDS target low voltage high current PDSs. Such systems are extremely difficult to design and demand novel control and converter topologies for efficient operation. On the other hand, a high voltage AC, low current system can be easily realized in HFAC system by using a simple HF transformer that easily steps up the voltage. This helps in minimizing the copper loss.
- Improved reliability with the number of power conversion operations decreasing thereby decreasing the semiconductor components
- Galvanic isolation with high frequency transformer
- DCPDS show poor dynamic response in comparison with HFAC PDS
- Higher power density owing to high frequency operation.

In spite of several exceptional advantages, there are a few drawbacks to the system as well, listed out below –

- Higher Electromagnetic Interference (EMI) effect hinders HFAC applications
- At high frequencies, skin and proximity effects increases leading to more loss.
- High frequency power distribution amplifies impedance in the transmission line which makes it difficult to transmit power
- Connecting high frequency inverters in parallel to realize higher power is difficult due to difference in phases of voltage.

This design paper discusses the advantages of employing HFAC PDS systems on aircraft and also explores the idea of switched capacitor and switched inductor based converters' role in designing multi-level voltage source and current source inverters respectively, for more electric aircrafts. Switched inductor converters can be derived using duality principle introduced by Prof. Cheng [4]. Switched inductor based converters are an attractive solution to be used current source inverters. Section II introduces aircraft power system standards and discusses about the existing aircraft power system and suggests improvement on the same. Section III looks into HFAC multilevel inverters employing switched capacitor and possibly switched inductor topologies. Concluding remarks are given in section IV.

II. POWER SYSTEM IN AIRCRAFTS

The power system design and components of an aircraft must be extremely robust and must meet certain stringent standards before they are allowed to be employed onboard. Some of the important standards include:

1. MIL-STD-704F – This standard focuses on the quality of electric power at the input terminals of the utilization equipment. However, this does not include EMI issues [5]
2. MIL-STD-461E – This standard is to control EMI characteristics of electrical equipment of aircraft. [6]
3. MIL-STD-810F – This looks into the stresses that the materials are under during the service period and material system performance requirements [7].
4. MIL-STD-1275D – This standard covers regulations for the 28 V DC power distribution systems in military vehicles including aircraft [8].

All the standards listed above are developed by the team of researchers from the department of defense, USA. The main focus of the standards is to ensure safety and compatibility among different systems onboard. All systems for an aircraft have to pass several such standards before they are employed in the aircraft.

Conventional power distribution system of an aircraft is shown in Fig. 3. With advances in enabling technologies

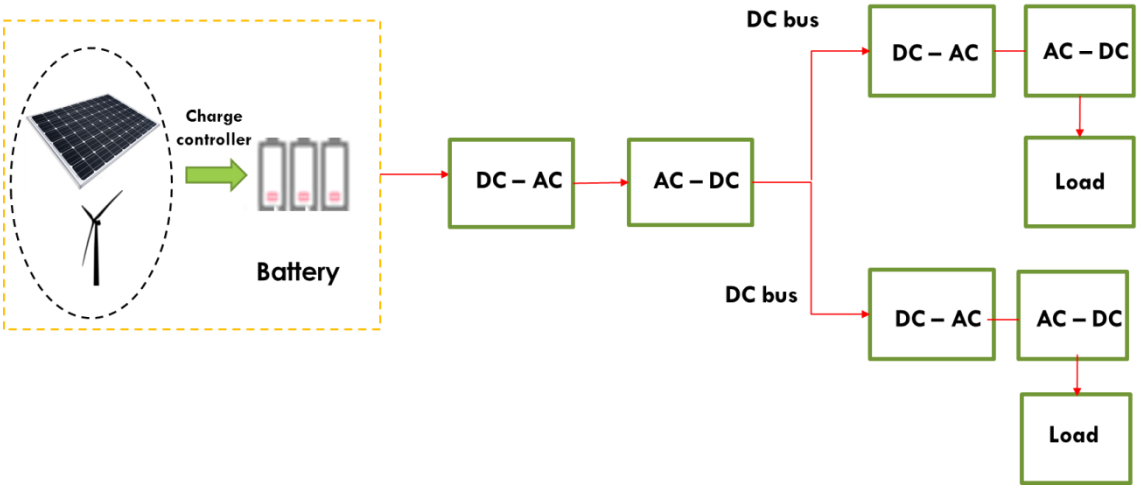

Fig. 1. General DC Power Distribution Architecture

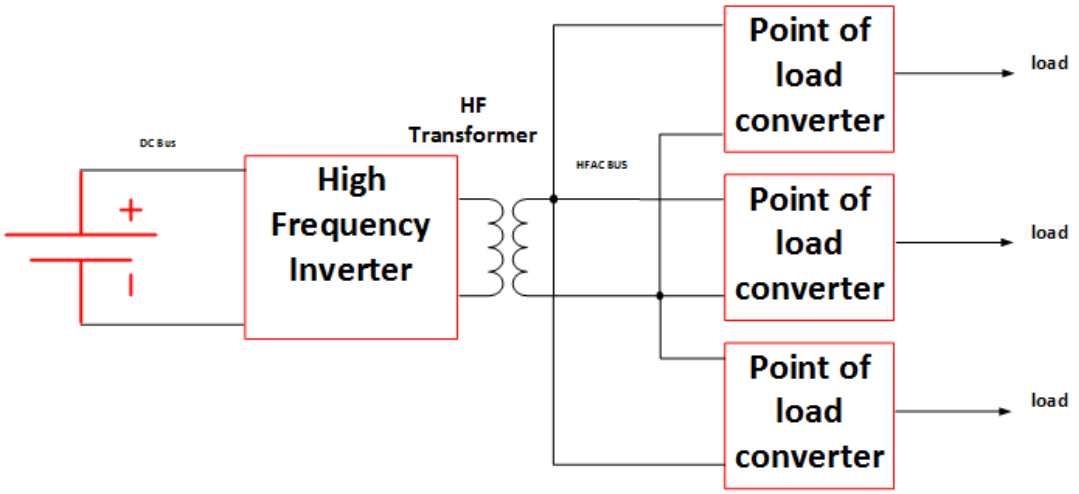

Fig. 2. HFAC Power Distribution Architecture

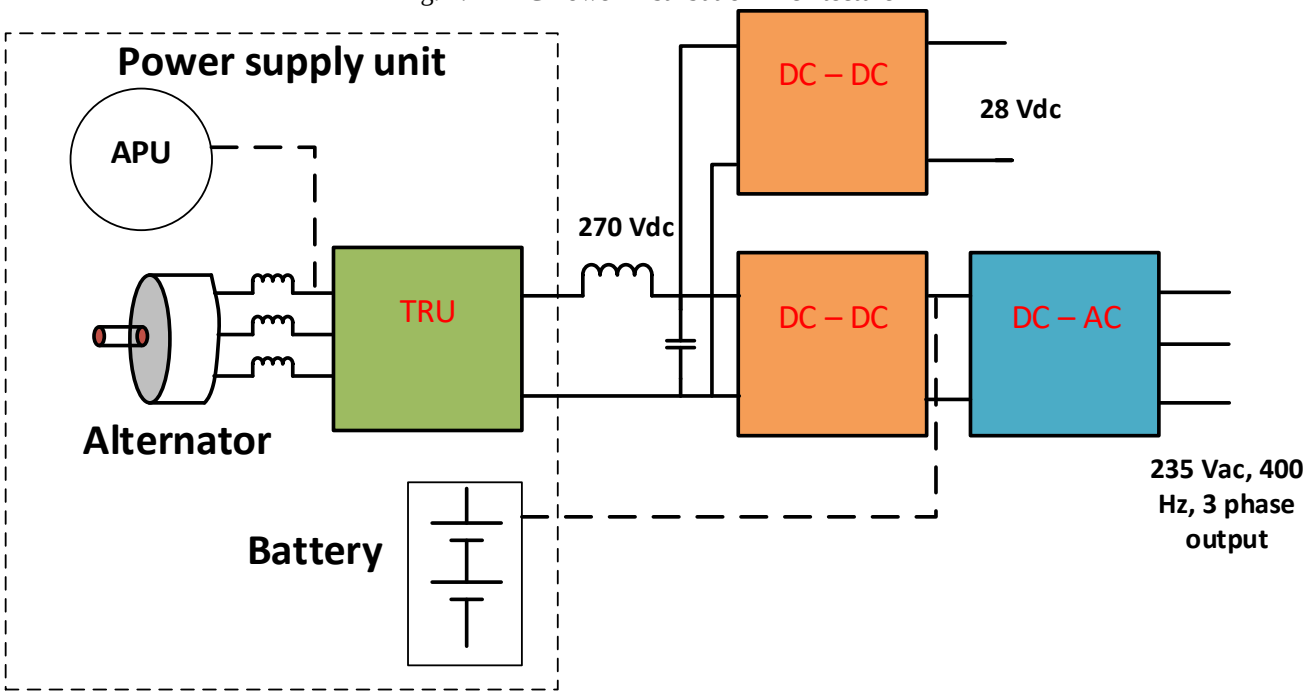

Fig. 3. Present aircraft electrical power system unit

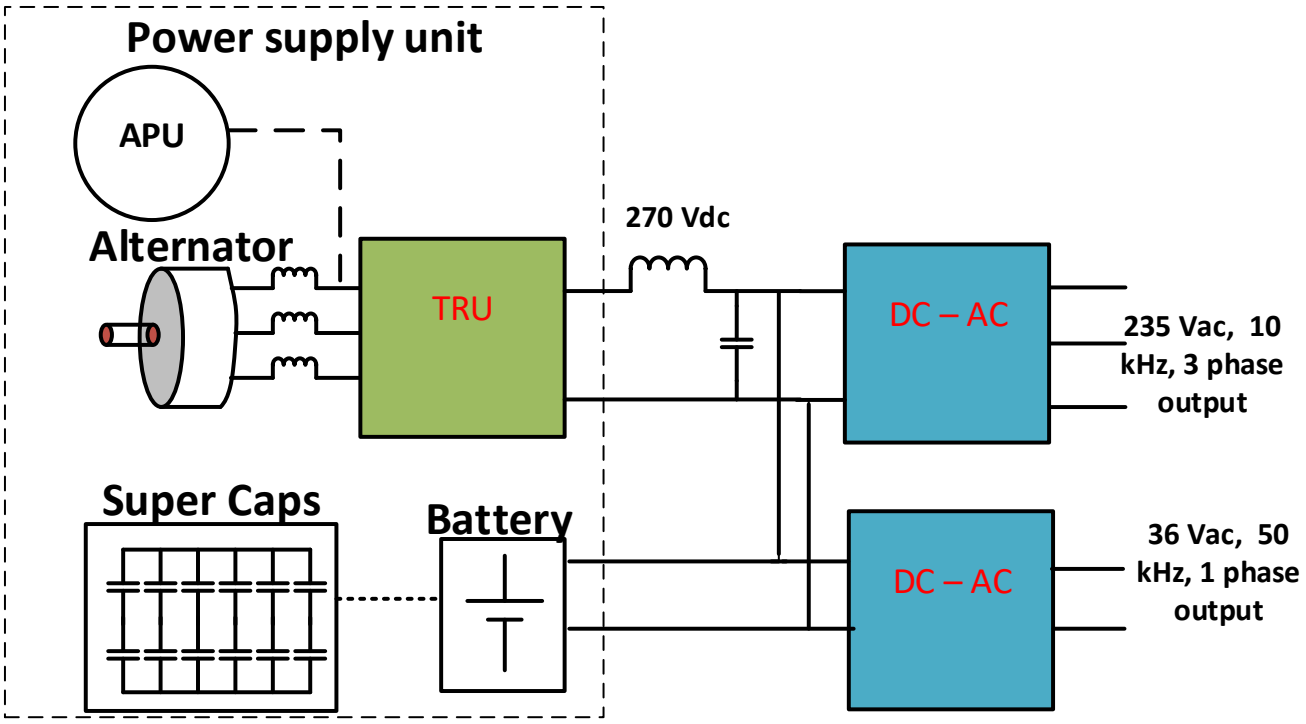

Fig. 4 Proposed electrical system architecture

like power electronics, motor drives, improved thermal management and better materials, all electric aircrafts will soon be a possibility. All electric aircrafts offer improved efficiency, reduction in cost, better reliability, maintenance, improved reliability, batter maneuvering capabilities, enhanced safety and greener systems. A recent example is the electrical system of Boeing's 787 dreamliner [9] [10].

From Fig. 3, it can be observed that the maximum distribution frequency is 400 Hz. There have been several papers on higher frequency range of power distribution for telecommunication, computer power supply, vehicular auxiliary power supply and micro grid applications [3]. It is imperative that we employ such systems inside aircraft for aforementioned advantages. The proposed system, in Fig. 4, replaces 28 Vdc system with a 36 V, 50 kHz power distribution system. The entire aircraft power distribution now is HFAC. This helps in higher power density operation which helps in reducing fuel consumption. HFAC operation, higher than 10 kHz, is safer for human than DC [11].

The new design also incorporates super capacitors into the system. The main purpose of introducing super capacitors is for its high power density. It can be extremely useful during starting of engine where traditionally bulky batteries are used. Additionally, super capacitors are much safer than batteries as they utilize electric field whereas batteries use chemical reaction for energy conversion. Due to the same reason, super capacitors have quicker response time in comparison to batteries. Ideally, one can expect a battery free future electric aircraft. However, this is possible only if research leads us to high energy density super capacitors or reliable fuel cell technology.

Super capacitors also play a crucial role in tapping the regenerative energy when the aircraft lands. Enormous weight thrusts onto the ground and this energy can be used by using the principle of regeneration of motors. Safe energy harvesting on a large scale is possible by employing large super capacitor banks that can sink in high magnitudes of current. This system design is not easy with only batteries as the power source as batteries have lower charging current rating in comparison with super capacitors and therefore all energy regenerated may not be successfully stored.

III. HF Multilevel Inverters

There are plethora of advantages that multilevel inverters offer in comparison to traditional ones [11][12]. In general, they include –

1. Better quality output voltage with lower distortions and *dv/dt.*
2. Input current drawn has low distortion.
3. Lower voltage rating and stress on semiconductor switches

HFAC multilevel inverters are possible by using simple switched capacitor techniques as elaborated in [13][14]. These inverters fully utilize the features of multilevel inverters and apply it to high frequency power distribution systems. These multilevel HFAC inverters can be employed in aircraft systems. A distributed power system consisting of several inverters to cater to different areas of the aircraft loads under a unified controller for the entire aircraft would be a novel and practical design. Using the duality principle [4], future electric aircraft with solar panels embedded onto them can employ multilevel high frequency switched inductor based current source inverters. An example of switched inductor based multilevel CSI derived from switched capacitor based has been shown in Fig.5.

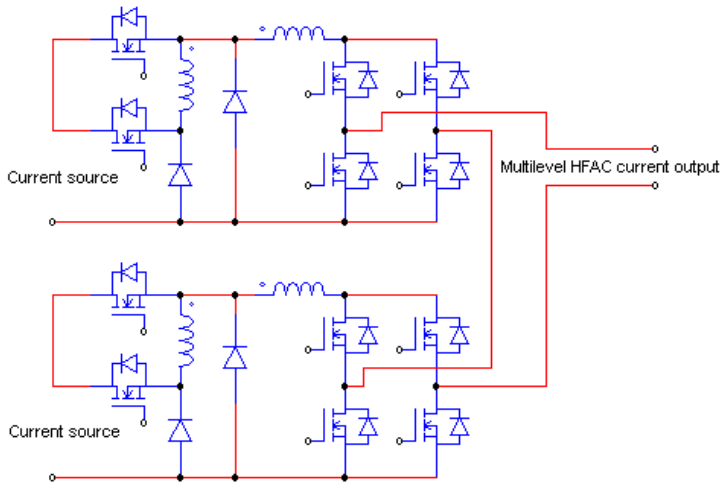

Fig. 5 HFAC 9-level switched inductor based CSI derived from switch cap based from [14] using duality principle

IV. Conclusion

This competition paper focuses on simple ideas to improve the existing electrical system of an aircraft and supports the global initiative for more / all electric aircrafts in future. The paper discusses the possibility of HFAC power distribution systems inside the aircraft to utilize several benefits it offers. Incorporating super-capacitors into the system offers several advantages during starting and regenerative braking. Multilevel switched capacitor and switched inductor based HFAC VSI and CSI respectively offer good features that improve the overall design of the power distribution system in an aircraft.

References

[1] Status of 20 kHz Space Station Power Distribution Technology. NASA Publication, TM 100781.

[2] Renz, David D., et al. Design considerations for large space electric power systems. No. N-8324552; NASA-TM-83064; E-1535. National Aeronautics and Space Administration, Cleveland, OH (USA). Lewis Research Center, 1983.

[3] Jain, P.; Pahlevaninezhad, M.; Pan, S.; Drobnik, J., "A Review of High-Frequency Power Distribution Systems: For Space, Telecommunication, and Computer Applications," in Power Electronics, IEEE Transactions on , vol.29, no.8, pp.3852-3863, Aug. 2014.

[4] Cheng, K.W.E.; Yuan-mao Ye, "Duality approach to the study of switched-inductor power converters and its higher-order variations," in Power Electronics, IET , vol.8, no.4, pp.489-496, 4 2015

[5] URL - http://everyspec.com/MIL-STD/MIL-STD-0700-0799/MIL_STD_704_1080/ (Last accessed 15th Oct 2015)

[6] URL - http://everyspec.com/MIL-STD/MIL-STD-0300-0499/MIL-STD-461E_8676/ (Last accessed 15th Oct 2015)

[7] URL - http://everyspec.com/MIL-STD/MIL-STD-0800-0899/MIL_STD_810F_949/ (Last accessed 15th Oct 2015)

[8] URL - http://everyspec.com/MIL-STD/MIL-STD-1100-1299/MIL-STD-1275D_5431/ (Last accessed 15th Oct 2015)

[9] URL - (Last accessed 15th Oct 2015) http://www.boeing.com/commercial/aeromagazine/articles/qtr_4_06/article_04_3.html

[10] URL - (Last accessed 15th Oct 2015) http://www.boeing.com/commercial/aeromagazine/articles/qtr_4_07/article_02_3.html

[10] Patel, Mukund R. Spacecraft power systems. CRC press, 2004, ch. 22, sec. 22.7, pp. 539-543.

[11] Kouro, Samir, et al. "Recent advances and industrial applications of multilevel converters." Industrial Electronics, IEEE Transactions on 57.8 (2010): 2553-2580.

[12] Rodriguez, Jose, Jih-Sheng Lai, and Fang Zheng Peng. "Multilevel inverters: a survey of topologies, controls, and applications." Industrial Electronics, IEEE Transactions on 49.4 (2002): 724-738.

[13] Ye, Yuanmao, et al. "A Step-Up Switched-Capacitor Multilevel Inverter With Self-Voltage Balancing." Industrial Electronics, IEEE Transactions on 61.12 (2014): 6672-6680.

[14] Liu, Junfeng, K. W. E. Cheng, and Yuanmao Ye. "A cascaded multilevel inverter based on switched-capacitor for high-frequency AC power distribution system." Power Electronics, IEEE Transactions on 29.8 (2014): 4219-4230.

A New Two-degree of Freedom switched Reluctance Motor for Electric Vessel

S. Y. Li K. WE. Cheng N.C. Cheung

[1,2, 3]Power Electronics Research Centre, Department of Electrical Engineering, The Hong Kong Polytechnic University, Hong Kong

Abstract - This paper introduces a new 2-degree of freedom (2-DOF) switched reluctance motor for an electric vessel. The configuration, operation principle and algorithm of the new motor are described in detail. Moreover, the electromagnetic characteristics have been illustrated by using finite element method (FEM), and the simulation of the electric vessel also has been realized. A modified control method has been suggested as the control scheme to ensure innovation and stability of the electric vessel's operation. Finally, the experimental results have suggested that the innovation and conveniences of the new electric vessel are better than that of conventional electric vessel, then the results of theoretical analysis and experiments has been proved the improvements of the electric vessel.

Index Terms—2-DOF, switched reluctance motor, electric vessel, FEM

I. INTRODUCTION

Electric vessel, as a new type of electrical propulsion transportation, has been investigated for years. The motors are practically used for the high power transportations with a high degree of reliability, such as electrical vehicles, aircrafts and electric vessel.

A two - dimensional rotating linear motor is usually used for the industrial motion control equipment. The two-degree switched reluctance motor is an alternative to be selected to drive this motion, such as boring mill, drill press and carving machine, etc [1].

The two-degree motions are required in surface motion or multi-axis applications, such as concentrating photovoltaic generation system in capturing the solar direct light to enhance power generation efficiency. The solar tracking is 2-dimension as the solar path varies throughout a year. Conventional 2-degree of freedom motions are realized by combining two rotary or linear (RL) motors in two directions, integrating screw rods and mechanical gears. For example, helical motion induction machines are reported in ref [2] and [3]. By using those mechanical gears, both the position precision and efficiency of the motion system could be reduced because there are backlash, axis-coordination and losses generated by mechanical gears. This 2-degree switched reluctance motor can realize two-degree movements-rotary and linear movements, directly, which is similar to the multilayer SR motor reported in [4]. This proposed direct-drive scheme is able to solve the problem of the low efficiency and position control caused by backlash and extra mechanical losses in conventional 2-degree of freedom motion platform and hence the whole system efficiency is significantly improved.

In addition, due to the simple mechanical structure of the proposed 2-degree of freedom switched reluctance motor characterized by low cost, high robustness, variable speed regulation, etc., the cost of the whole system could be reduced. Meanwhile, the 2-degree of freedom switched reluctance motor can operate well under high temperature as well as deteriorated working environment because this motor has no permanent magnet.

The invention is the 2-degree of freedom switched reluctance actuator that consists of the frame, stator cores, stator coils, mover cores, air gaps between the stator poles and the mover poles, and the mover shaft, that integrates the longitudinal magnetic structure with the transverse magnetic structure, and relates to electromagnetic rotary-linear actuators. Besides, combining pole structure and small tooth structure can further enhance the efficiency of the rotary-linear actuator that can realize linear motion and rotary motion simultaneously.

The traditional form of rotating linear motion adopts two rotating motors or the combination of a linear motor and a rotating motor for implementation [5]-[7]. However, this combination not only increases size and weight of the drive, but also reduces working accuracy of the equipment. Therefore, to explore an integrated rotating linear motor, an optimized rotary-linear motor based on switched reluctance principle is presented. The structure of the motor for the vessel electrical propulsion system is also discussed and the structure of the motor is optimized in this paper. Until now, the integrated rotating linear motor is based on switched reluctance principle, which has been preliminary researched. A rotating linear switched reluctance motor presented in [8], is to integrate rotating motion and linear motion based on the minimum reluctance principle, while to achieve rotating linear motion, and to reduce volume of the driver and increase accurate position control. However, the coupling of this linear motor has occurred when both rotating motion and linear motion, and the motion of rotating and linear are produced by the same coils, so the motor will produce unwanted linear directional force upon the movement of rotating motion, and vice versa. A method of decoupling control for the reduction of coupling effect of the motor's operation has been proposed [9]; to excite reasonable distribution control current of the motor stator coil, and the decoupling of both rotating motion and linear motion have been implemented. Therefore, the control accuracy has been improved. Since the motor is based on the principle of switched reluctance, so the efficiency of switched reluctance is lower than other motors, and the force volume ratio is relatively poor [10]. Even the rotating linear motor has been controlled by the method of the decoupling, but cannot solve the problems of the lower

conversion efficiency, the smaller torque and linear direction force [11], [12].

The paper presents an optimized rotating linear motor, and it is applied to the electric vessel. In the paper, firstly, a new structure of the motor is proposed. The mathematical model of the two - dimensional rotating linear is established. Secondly, through the finite element analysis of the motor, internal electromagnetic field distributions of the motor and force characteristics of the motor are obtained. Experiments are carried out to study the accurate control of motor. Thirdly, to control the position of motor and to realize the angle and position control, an optimization is needed to resolve the electrical propulsion performance, and also to improve the force to volume ratio.

II.CONSTRUCTION OF THE SYSTEM

A. Mechanical structure and basic control method of the electrical propulsion system

The new electrical propulsion system is only based on one two-degree switched reluctance motor to complete all propulsion operation, the two-degree switched reluctance motor have connected with propellers, which is shown in Fig.1. Therefore, in the Fig.2, the direction control is achieved by the linear motion of the motor and the linear acceleration control is achieved by the rotating motion of the motor. To compare with traditional electric vessel propulsion system, not only the operation of electric vessel is more hommization and convenience, but also the operation precision is improved. The electric vessel is readily for industrialized production.

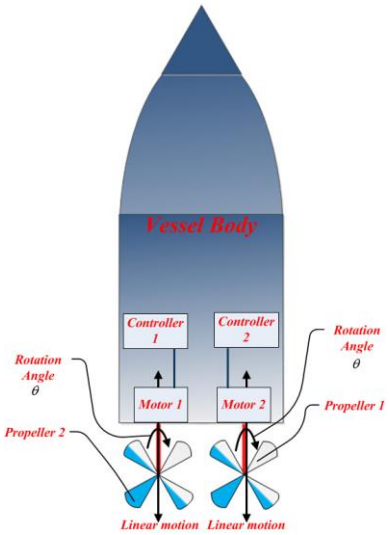

Fig.1 Mechanical structure of the electrical propulsion system

B. Actual structure of the motor

Fig.3 (a) is the mechanical configuration of the two degrees of freedom switched reluctance motor; Fig. 3 (a) is left view of the motor. It mainly consists of a linear guider, the first part and the second part. Both parts have teeth and slots. When each phase is excited, the second part will rotate to the position at which all teeth of the two parts are directly opposite. Fig.3 (b) is front view for the motor. As shown in the figure, the first part has three phases named as phase A, B and C, respectively. The second part has five units fixed on the linear guider. Two bearings are used to guider the movements of the second part both in rotary and linear directions. When phase A is excited, the second part will shift to left. Also, if phase C is excited, it will move to right. Therefore, the second part can realize linear motion to left by exciting phase A, C and B in sequence. The main specifications are listed in Table I.

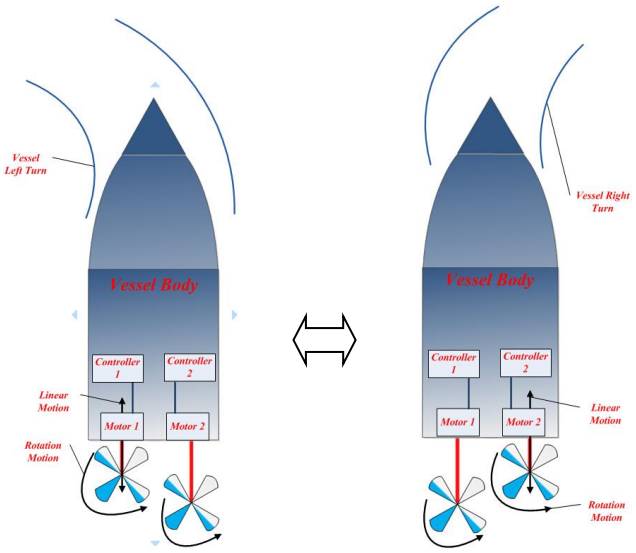

Fig.1 Basic control method of the electrical propulsion system

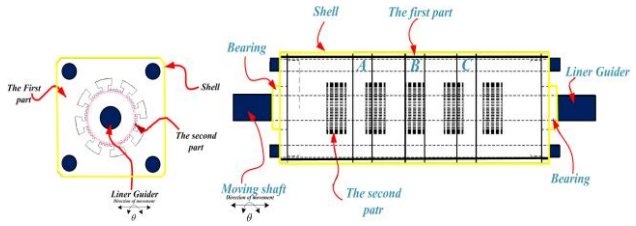

(a) (b)

Fig.3 The mechanical configuration of motor

The magnetic field generated by the concentrated coils passing current, rounding the core in the first part, attracts the second part. Based on the minimum reluctance principle, a unit of the second part will move to the position, which has the minimum reluctance, thus producing electromagnetic propulsion or torque. By controlling currents passing in the coils of the first part, the generated propulsion and torque will drive the second part and then it will realize rotary and linear motions simultaneously. As shown in Fig.3 (b), when the second part shifts linearly, phases A, B and C should be excited in turns. For example, phase B is totally aligned in the figure. At the position the second part would move left if phases A, C and B are excited in sequence and vise versa. For the first part, there are several small teeth in each pole and there are eight poles of each phase of the motor. The working rules probably the same as common switched reluctance drives, namely through controlling the ON/OFF conditions of the first pole. All of A, B and C phrase positions were fixed with one shaft, which would be led by two bearings in order to realize linear and rotational motions.

1) *Mathematic mode*

Equation (1) is the voltage equation for both rotary and linear parts [13].

$$V_\mu = R_\mu I_\mu + \frac{f_\mu dv}{dt} \tag{1}$$

And V_μ is the input voltage and I_μ is current for the u^{th} coil (u is1-6). R_μ is winding resistance for the coil, and f_μ is flux-linkage confirmed during excitation.

The rotary-linear machine consists of a coupled RL electromechanical system. From the rotary part with each stator ring, and equation (2) is the machine generalized torque characteristic T as,

$$T = Q\ddot{\theta} + G\dot{\theta} + T_L \tag{2}$$

where the moment of inertia is Q , rotational friction coefficient is G . Angular position is θ and load torque is T_L . For the linear motion, the generated force F is

$$F = S\ddot{z} + N\dot{z} + F_L \tag{3}$$

whereas mass of the moving shaft is m , and linear friction factor is L . The linear position and thrust force are x and F_L , respectively. Assume the magnetic circuit is not saturated in the linear motion region. Toward the phase inductance, the influence can be neglected for the phase current [22], also force can be estimated as,

$$\begin{cases} T = \frac{1}{2}\cdot\frac{\partial L_1}{\partial \theta}\cdot i_1^2 + \frac{1}{2}\cdot\frac{\partial L_2}{\partial \theta}\cdot i_2^2 \\ F = \frac{1}{2}\cdot\frac{\partial L_1}{\partial x}\cdot i_1^2 + \frac{1}{2}\cdot\frac{\partial L_2}{\partial x}\cdot i_2^2 \end{cases} \tag{4}$$

And L_1 and L_2 are total inductances, and i_1 and i_2 are the two stator rings current, respectively. It can be found that the torque and force generation are both dependent on phase current of the stators. The stator ring for linear motion in the mean time can generate the torque. Consequently, the magnetic paths are nonlinear and highly coupled.

2) *Electromagnetic characteristics*

In order to analyze the magnetic field distribution and properties of the motor, FEM is employed. The mesh model of the motor as shown in Fig.4, actually, it is a model with symmetrical structure, which subdivides the computational nodes and reduces calculation time. It can be concluded from the figure, subdivision of the air gap between two parts is intensive, and the more unions of subdivision were set, the higher quality of computation could be obtained.

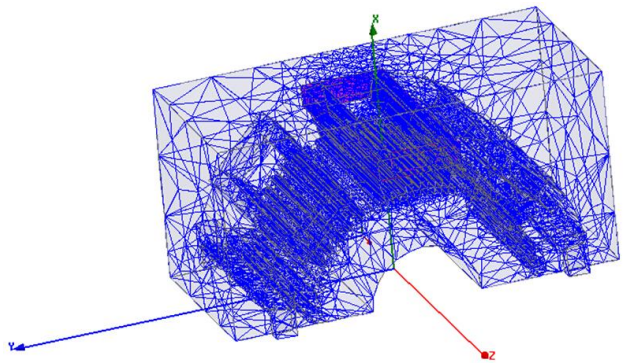

Fig.4 is the distribution of magnetic flux lines in the motor

When it works, it is clear to see that the electromagnetic torque or propulsion is produced when the magnetic flux lines are closed from the first part to the second. The flux linkage will be built when the coils are excited. When the motor moves, the magnetic lineation of the field coil is in the same flat with the second part. Fig.5 describes the distribution of magnetic lineation when the second part moves in the position that is not aligned with the first part. When the motor works in the linear direction, magnetic flux line is vertical with the direction of the linear direction, which is different from the principle of producing tension when the motor moves. So the motor can produce not only torque, but also the propulsion in the linear direction, thus decreasing the volume of the two dimensional motions actuators and simplifying the execute components. In addition, there is no need to add any intermediate mechanical converters because both of the torque and linear propulsion of the motor are direct-drive mode, which can realize the precise position control.

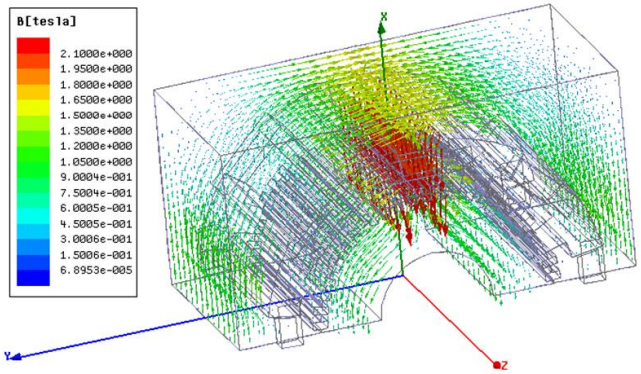

Fig.5Magnetic field distribution of the motor in rotary direction

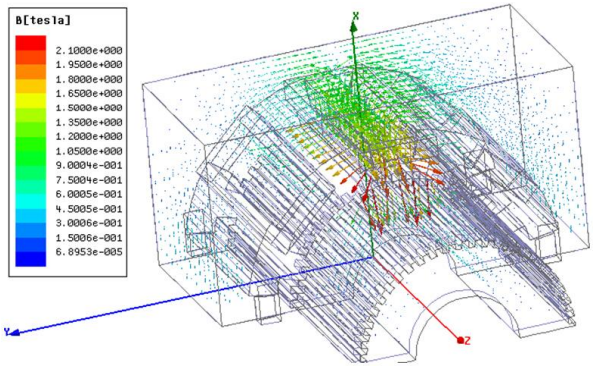

Fig.6 Magnetic field distribution of the motor in linear direction

From the distribution of magnetic field, the rectilinear motion of the motor and the magnetic field both come

from the same coil, thus, the motor in rectilinear motion will produce the torque of rotational motion. There is coupling between them, however, it is acceptable to avoid the coupling by a kind of decoupling controlling method, in order to realize the high quality controlling.

Fig.7 and Fig.8 are the waveforms of FEM calculation from the torque and rectilinear directions. Fig.7 is the waveform of measured torque data. Any phrase position excites, the maximal torque is 0.71N.m, and the torque will not increase accordingly under large current, because the motor has saturated, the permeability of magnetic material and the volume of motor limit the increase in magnetic field intensity, which can make the increase in torque inconspicuous.

TheFig.8,that the propulsion of the motor is increased with therising of phase current because it is hard to reach the sa turated point to the motor as it moves from unaligned Posit ionton aligned position, during which the reluctance is big enough. This figure shows the propulsion profiles corresponding to all positions during a stroke. The linear propulsion is relatively low and up to 10N at the rate current.

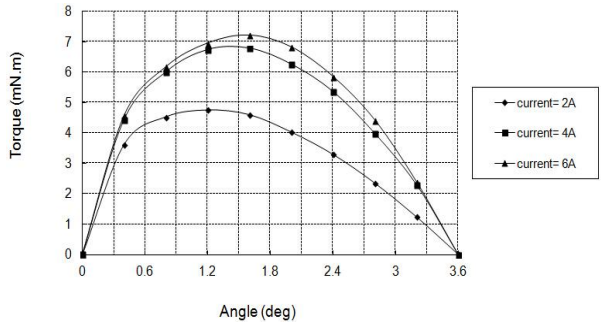

Fig.7 Torque output with different currents

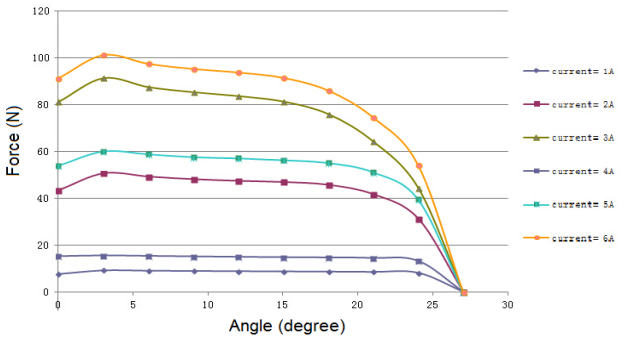

Fig.8 Force output profiles corresponding to position

From the analysis above, this two-degree of freedom stabilized platform motor can directly realize the motions of linear and rotary movements.

III. POSITION CONTROLLER DESIGN FOR THE TRACKER

Two PID controllers are employed for linear and rotary motions [14] for the tracking system and the whole control scheme is expressed in Fig.9.

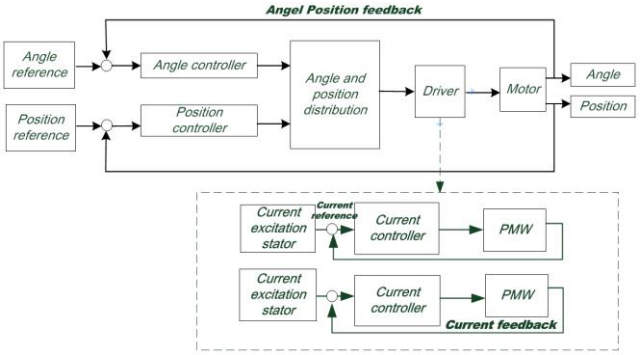

Fig.9 Control block of the motor

The control system is divided into two parts. On one hand, a controller regulates the linear motion whose axis is responsible for the perpendicular motion for the electric vessel. On the other hand, another controller gives the horizontal movements for the system controls in rotary motion. The feedbacks of both the two axis positions of angle and linear displacement are sampled by a sensor which tracks movements of the sun. Controllers output the force and torque reference commands for the force to current and torque to current distribution parts [15]-[17]. Finally, the two distribution parts output current commands for the divers to the motor. The trajectories of the two axes for the motor are obtained in the end as shown in Fig.9. The simple PID controller can be applied in angular and linear position control with control parameters in Table I.

Table I. Parameters of position controllers

Parameters controller	Angular position controller	Linear position controller
P	0.410	32.5
I	6.006	2.2
D	0.005	0.008

IV. EXPERIMENTAL RESULTS

The achievements of experimental is shown in Fig.10, with A DSPACE DS1104 controller card, the encoders collect the position feedback with two channels of quadrature encoder pulse interface, also for each stator, the controller card generates the current reference of any phase. Lastly, the six current drivers generate the phase current outputs.

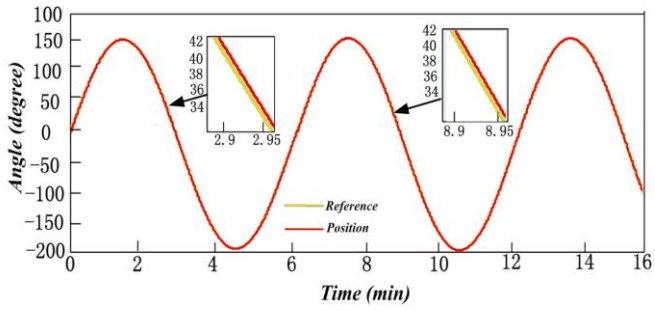

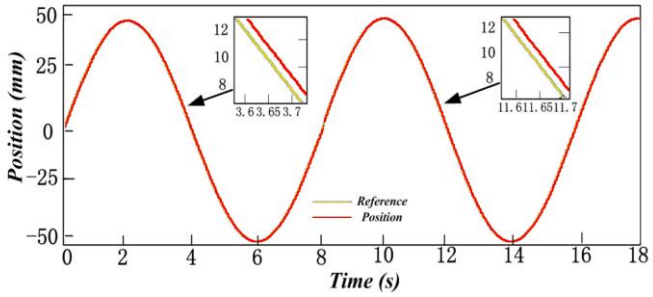

(a)

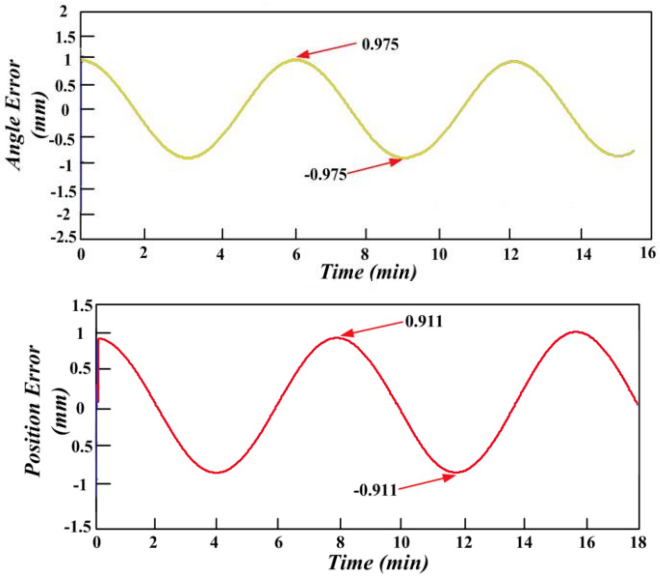

(b)

Fig.10(a) Position control performance for rotary and linear motion (b) Dynamic error response

In Fig.10 (a) and (b) proved the position control performance and the theory of dynamic tracking error response. The results shows that the proposed two-degree freedom of SR motor not only has a high position tracking precision of less than 0.4°, but also the performance of the period of working is stable and reliable. Consequently, the achievements of theory analysis and FEM have been proved by the improvements of the proposed setup

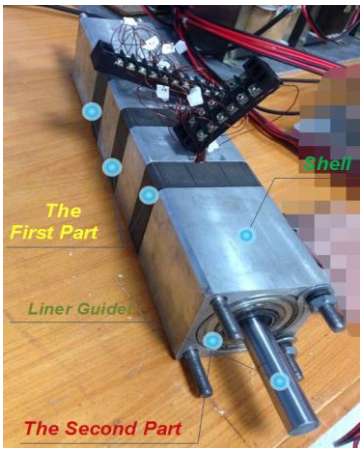

(a)

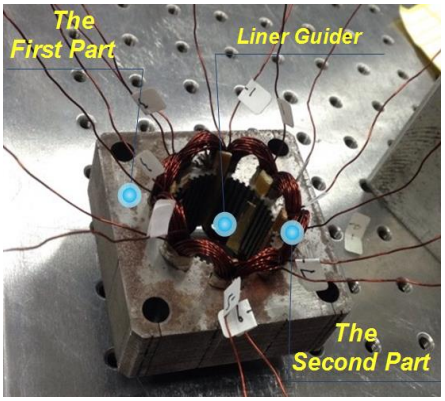

(b)

Fig.10 (a) and (b) are the prototype of the 2-degree freedom of SR motor

The structure of the proposed motor is shown in (b) and (C), its features and operated performance have been discussed in detail above.

V. Conclusion

This paper proposed a modified electric vessel based a new 2-degree of freedom SR motor, also its analysis of theory, configuration and control method are described in detail. Lastly, the achievements of experiment have proved the improvements of the modified electrical propulsion system of the vessel. Using a 2-degree SR motor to replace the two conventional motors is novel for such application. The proposed electric vessel is not only simplifying the operation method, also promoting the direction precision. Consequently, the experiment has proved the improvements of the system, and it will be used for wider industrial applications with its attractive superiority.

Reference

[1] G. Krebs, A. Tounzi, B. Pauwels, D. Willemot, and F. Piriou, “Modeling of a linear and rotary permanent magnet actuator,” IEEE Trans. Magn., vol. 44, no. 11, pp. 4357–4360, Nov. 2008.

[2] T. Onuki, et al., "Induction motor with helical motion by phase control," IEEE Transactions on Magnetics, vol. 33, pp. 4218-4220, 1997.

[3] J. Alwash, et al., "Helical motion tubular induction motor," IEEE Transactions on Energy Conversion, vol. 18, pp. 362-369, 2003.

[4] E.S. Afjei and H.A. Toliyat, "A novel multilayer switched reluctance motor," IEEE Transactions on Energy Conversion, vol. 17, pp. 217-221, 2002.

[5] C. T. Liu and T. S. Chiang, “Design and performance evaluation of a microlinear switched-reluctance motor,” IEEE Trans. Magn., vol. 40, no. 2, pp. 806–809, Mar. 2004.

[6] Y. Sato, “Development of a 2-degree-of freedom rotational / linear switched reluctance motor,” IEEE Trans. Magn., vol.43, no.6, 2007, pp.2564-2566

[7] Pan, Yu Zou, Cheng. N. C, “Performance analysis and decoupling control of an integrated rotary–linear machine with coupled magnetic paths”, IEEE Transactions on Magnetics, Vol. 50, Issue: 2, 2014

[8] X.D. Xue, K.W.E. Cheng and S.L. Ho, “Influences of output and Control Parameters on Power Factor of Switched Reluctance Motor Drive Systems”, Electric Power Components and Systems, Dec 2004, Vol. 32, No. 12, pp. 1207-1223.

[9] X.D. Xue, K.W.E. Cheng and S.L. Ho, “Improvement of power factor in switched reluctance motor drives through optimizing in switching angles”, Electric Power Components and Systems., Dec 2004, Vol. 32, No. 12, pp. 1225-1238.

[10] X.D. Xue , K.W.E. Cheng and S.L. Ho, "Simulation of Switched Reluctance Motor Drives Using Two-dimensional Bicubic Spline", IEEE Tran. Energy Conversion. Dec 2002, Vol. 17, Issue 4, pp. 471-477.
[11] Y. -C. Lai, Y. -L. Lee, and J. -Y. Yen, "Design and servo control of a single-deck planar maglev stage," IEEE Trans. Magn., vol. 43, no. 6, pp. 2600–2602, Jun. 2007
[12] G. Li, J. Ojeda, S. Hlioui, E. Hoang, M. Lecrivain, and M. Gabsi, "Modification in rotor pole geometry of mutually coupled switched reluctance machine for torque ripple mitigating," IEEE Trans. Magn., vol. 48, no. 6, pp. 2025–2034, Jun. 2012.
[13] X.D. Xue, K.W.E. Cheng and S.L. Ho, "Improvement of power factor in switched reluctance motor drives through optimizing in switching angles", Electric Power Components and Systems., Dec 2004, Vol. 32, No. 12, pp. 1225-1238.
[14] M. Bodson, J. Chiasson, R. Novotnak, and R. Ftekowski, "High-per-formance nonlinear feed back control of a permanent magnet stepper motor," IEEE Trans. Control Syst. Technol. , vol. 1, no. 1, pp. 5–14, Mar. 1993.
[15] D. Chen and B. Paden, "Adaptive linearization of hybrid step motors: Stability analysis," IEEE Trans. Autom. Control, vol. 38, no. 6, pp. 874–887, Jun. 1993.
[16] S. A. Stuart, J. E. McInroy, and R. M. Lofthus, "Closed loop low- velocity regulation of hybrid stepping motors amidst torque distur- bances," IEEE Trans. Ind. Electron. , vol. 42, no. 3, pp. 316–324, Jun. 1995.

Author Index

Submission Details

Only online submission will be accepted. Please first register and submit online. The paper is in double column and is similar to most IET or IEEE journal format. There is no page limit. Any number of pages of more than 6 will be subject to additional charge.

The paper guidelines can be downloaded using the link: http://perc.polyu.edu.hk/apejournal/

Any queries, please contact Prof. Eric Cheng, Publishing Director of APEJ, Dept. of Electrical Engineering, The Hong Kong Polytechnic University, Hung Hom, Hong Kong. Email: eeecheng@polyu.edu.hk Fax: +852-2330 1544

Any secretarial support and production related matters, please contact Dr. James Ho, Power Electronics Research Centre, The Hong Kong Polytechnic University, Hung Hom, Hong Kong. Email: eeapej@polyu.edu.hk Tel: +852-3400 3348 Fax: +852-3400 3343

Publication Details

The Journal will be published 2-3 times a year. The first issue was published in 2007. Response time for paper acceptance is within 3 months.

Financial Charge

All the accepted papers will be printed without charge for 6 or less pages. An additional page charge is HK$100 per page. A hardcopy of the journal will be posted to the corresponding author free of charge. Additional copies of the journal can be purchased at HK$200 each. The charge includes postage and packing.

All Chinese Papers will be subjected to a translational fee of HK$350 per page. It will be charged when the paper is accepted for publication.

Advertising

Advertisement is welcome. Full page advertisement is HK$1000. For colour advertisement, the amount is doubled. All the advertisement will be both posted online in the journal website and hardcopy of the journal.

For advertising enquiries and details, please contact Ms. Anna Chang, eeapej@polyu.edu.hk .
Tel: +852-3400 3348 Fax: +852-3400 3343

For payment, please send your cheque, payable to ‘The Hong Kong Polytechnic University, address to Ms. Kit Chan, Secretary of APEJ, Dept. of Electrical Engineering, The Hong Kong Polytechnic University, Hung Hom, Hong Kong.